Pergamon

Geochimica et Cosmochimica Acta, Vol. 67, No. 17, pp. 3165–3179, 2003

0016-7037/03 $30.00 + .00

doi:10.1016/S0016-7037(02)01298-X

Extinct ^{10}Be in Type A Calcium-Aluminum-Rich Inclusions from CV chondrites

GLENN J. MACPHERSON,[1,*] GARY R. HUSS,[2] and ANDREW M. DAVIS[3]

[1]Department of Mineral Sciences, Museum of Natural History, Smithsonian Institution, Washington, DC 20560-0119, USA
[2]Department of Geological Sciences and Center for Meteorite Studies, Arizona State University, Tempe, AZ 85287-1404, USA
[3]Enrico Fermi Institute and Department of the Geophysical Sciences, University of Chicago, 5640 S. Ellis Ave., Chicago, IL 60637, USA

(*Received November* 8, 2001; *accepted in revised form September* 19, 2002)

Abstract—We have found clear evidence of live ^{10}Be in five normal Type A Calcium-aluminum-rich inclusions (CAIs), one normal Type B CAI, and one FUN Type A CAI, all from CV3 chondrites. The $(^{10}Be/^{9}Be)_0$ ratios range from $\sim 0.36 \times 10^{-3}$ to $\sim 0.77 \times 10^{-3}$ and are similar to those found by previous workers. The $(^{10}Be/^{9}Be)_0$ ratios do not correlate in a temporal fashion with $(^{26}Al/^{27}Al)_0$, suggesting that ^{10}Be and ^{26}Al were produced by different mechanisms. An examination of possible sources for the short-lived radionuclides indicates that production of ^{10}Be was almost certainly by particle irradiation, possibly within the solar system, and was probably accompanied by significant production of ^{41}Ca and ^{53}Mn. In contrast, all of the ^{60}Fe, most of the ^{26}Al, and some of the ^{53}Mn were probably produced in stars and were imported into the solar system within presolar dust grains. *Copyright © 2003 Elsevier Ltd*

This paper is dedicated with great affection to Bob Clayton on the occasion of his retirement. His monumental and pioneering achievements in so many areas of cosmochemistry have been an inspiration to all of us, and his wise counsel has always been invaluable.

1. INTRODUCTION

Matter in the earliest solar system contained short-lived radioactive nuclides (e.g., ^{26}Al, ^{129}I, ^{41}Ca, ^{53}Mn; see recent summaries by Podosek and Nichols, 1997, and Goswami and Vanhala, 2000), whose former presence is indicated by detectable excesses of their respective daughter products within components of primitive chondritic meteorites. These nuclides are commonly interpreted as indigenous to the presolar matter that formed the solar system, and many detailed calculations suggest that most or all of these nuclides were derived ultimately from nucleosynthesis in one or more kinds of highly evolved stars (Podosek and Nichols, 1997; Cameron, 1993; Wasserburg et al., 1994; Cameron et al., 1995). However, the idea that short-lived radionuclides were produced by particle irradiation in the solar system (an early explanation for ^{26}Al; Heymann and Dziczkaniec, 1976) has experienced a revival in the context of an X-wind model for formation of CAIs and chondrules (Lee et al., 1998; Gounelle et al., 2001).

A new addition to the list of short-lived nuclides in the early solar system is ^{10}Be ($t_{1/2}$ = 1.5 My). McKeegan et al. (2000) demonstrated a linear correlation between excesses of ^{10}B (the daughter product of ^{10}Be decay) and Be/B ratios in minerals from an Allende Type B Calcium-aluminum-rich inclusion (CAI), suggesting in situ decay of ^{10}Be after the inclusion formed. The estimated initial abundance ratio, $(^{10}Be/^{9}Be)_0$, at the time of CAI formation was $\sim 0.9 \times 10^{-3}$. Except for ^{7}Li and ^{11}B, the isotopes of lithium, beryllium (including ^{10}Be), and boron are not produced in significant quantities in stars; instead, they are produced primarily by cosmic ray interactions in interstellar space and are consumed by low-temperature burning in stars (Reeves, 1994; Woosley and Weaver, 1995). Calculations indicate that the inferred $(^{10}Be/^{9}Be)_0$ for the Allende CAI measured by McKeegan et al. (2000) is too high to represent the ambient ^{10}Be/^{9}Be from cosmic ray interactions in interstellar space, implying ^{10}Be production through an enhanced source of cosmic rays (Gounelle et al., 2001; McKeegan et al., 2000). In contrast to ^{10}Be, McKeegan et al. (2000) and others (Goswami et al., 2001) have argued that ^{60}Fe and the inferred solar system abundance of ^{26}Al could not have been made by irradiation and require a nucleosynthetic source. This interpretation implies that ^{10}Be and ^{26}Al should be decoupled from one another in early solar system materials. Gounelle et al. (2001) reached the opposite conclusion, arguing that nearly all of the short-lived radionuclides (except ^{60}Fe) could have been produced via irradiation by solar particles in magnetic reconnection rings near the active early sun. The disagreement arises from the fact that the calculated production of different nuclides varies strongly with the details of the irradiation (Gounelle et al., 2001). Thus it remains uncertain whether or not to expect a correlation between ^{10}Be and ^{26}Al in CAIs.

Finally, ^{10}Be may provide a constraint on the origin of the so-called FUN CAIs (those with large *F*ractionation and *U*nidentified *N*uclear isotopic effects; Wasserburg et al., 1977). Because ^{10}Be must be produced by irradiation, there is no obvious reason for ^{10}Be to correlate with the endemic isotopic anomalies that characterize FUN CAIs. If FUN CAIs show systematically different beryllium-boron isotopic characteristics than "normal" CAIs, then the two populations of CAIs may have formed in different places. If not, then their differences can be ascribed primarily to differences in their precursor compositions.

Thus there is a clear need for extensive studies of correlations or lack thereof between ^{10}Be and other isotopic properties of CAIs. Additional data will help to determine how widespread ^{10}Be was in the early solar system, help to refine the initial abundance ratios, reveal potential variations among CAIs, constrain the locations where different types of CAIs

* Author to whom correspondence should be addressed (glenn@volcano.si.edu).

may have formed, and provide information on the effects of secondary processes on the ^{10}Be-^{10}B system.

In this study we analyzed beryllium-boron systematics in seven CAIs: six Type As (two from Vigarano and one each from Leoville, Allende, Efremovka, and Axtell), plus one Type B1 from Vigarano. Our study differs from that of McKeegan et al. (2000) in two ways. First, we focused on CAIs from the reduced-type CV3 meteorites (Vigarano, Leoville, and Efremovka) because CAIs in those meteorites generally lack the intense secondary mineralization that obscures primary features in CAIs from Allende and other oxidized-type CV3s. Secondary alteration zones in Allende CAIs are known to be enriched in boron relative to primary minerals (Davis et al., 1994; Davis, 2002). The CAIs studied by McKeegan et al. (2000) were all from Allende, although Sugiura et al. (2001) studied inclusions from Efremovka. The one Allende CAI that we did analyze, USNM 3898, is the CAI found by Gray et al. (1973) to have the lowest initial ^{87}Sr/^{86}Sr ratio of any solar system object ever measured. Second, we mainly analyzed Type A CAIs. Histograms of initial $(^{26}\mathrm{Al}/^{27}\mathrm{Al})_0$ ratios for Type A CAIs (MacPherson et al., 1995) show a single peak at $\sim 5 \times 10^{-5}$, whereas those for Type B CAIs also show a second peak at ~ 0. These data suggest that Type As have experienced less thermal reprocessing (isotopic resetting) than have the Type Bs and thus are likely to give a better indication of initial ^{10}Be/^{9}Be. One of the Type A inclusions we analyzed is a FUN inclusion (AXCAI 2771), which permits us to compare the beryllium-boron characteristics of normal and FUN CAIs.

For all of the objects we analyzed, aluminum-magnesium isotopic data either already existed or were collected during this work, allowing us to compare $(^{26}\mathrm{Al}/^{27}\mathrm{Al})_0$ with $(^{10}\mathrm{Be}/^{9}\mathrm{Be})_0$. Preliminary results of this work were reported in MacPherson and Huss (2001).

2. ANALYTICAL TECHNIQUES

2.1. Isotope Analyses

Analyses of magnesium isotopes were made with the new Cameca ims 6f ion microprobe at Arizona State University (ASU) and with the modified AEI IM-20 ion microprobe at the University of Chicago. Magnesium-aluminum measurements made at ASU were carried out using standard techniques (Fahey et al., 1987). A primary O^- beam of 0.05 to 0.5 nA (spots of 1 to 2 μm) was used, and the secondary mass spectrometer was operated at a mass resolving power of $\sim$3500, sufficient to completely resolve $^{24}MgH^+$ from $^{25}Mg^+$, $^{25}MgH^+$ from $^{26}Mg^+$, and $^{48}Ca^{2+}$ from $^{24}Mg^+$. To determine the excess at ^{26}Mg, a mass-fractionation-corrected ratio, $(^{26}\mathrm{Mg}/^{24}\mathrm{Mg})_{\mathrm{corr}}$, was calculated using a linear law (i.e., assuming that the fractionation for ^{26}Mg/^{24}Mg is twice that for ^{25}Mg/^{24}Mg). Shifts in ^{26}Mg/^{24}Mg remaining for sample minerals after accounting for both instrumental and intrinsic mass fractionation are reported in permil relative to terrestrial ^{26}Mg/^{24}Mg (Catanzaro et al., 1966):

$$\delta^{26}\mathrm{Mg} = \frac{(^{26}\mathrm{Mg}/^{24}\mathrm{Mg})_{\mathrm{corr}}}{0.13932} - 1) \times 1000$$

Differences in ionization efficiency between aluminum and magnesium were accounted for by comparing the measured $^{27}Al^+/^{24}Mg^+$ to the ^{27}Al/^{24}Mg ratio for each standard mineral.

Magnesium isotopes measured at the University of Chicago were measured using techniques summarized in Russell et al. (2000). Because the AEI IM-20 operates at a mass resolving power of $\sim$400, interference corrections are necessary. The interference from $^{48}Ca^{2+}$ on $^{24}Mg^+$ was monitored by measuring $^{40}Ca^{2+}$ at mass 20, and a small correction was made. The interference from $^{24}MgH^+$ on $^{25}Mg^+$ was minimized by cooling the ion extraction lenses with liquid nitrogen. No measurable interference was observed on standard minerals, so no corrections were made.

Lithium, beryllium, and boron analyses were carried out with the ASU ims 6f ion microprobe operating at a mass resolving power of $\sim$1800, sufficient to eliminate interferences from hydrides and multiply-charged ions. An imaged field of $\sim$50 μm was used to increase the fraction of the ions reaching the detector. To minimize boron contamination, a rastered area of 70 $\times$ 70 μm was sputtered around each spot until the boron count rate decreased to a low and relatively constant value. A 20–30 nA focused O^- beam, located at the center of the rastered area and masked by a field aperture (effective diameter $\sim$25 μm), was then used for the measurements. Energy scans were used to account (to first order) for charging of the sample surface during the analysis. Boron count rates were so low that the data were not collected as a series of ratio measurements, as is typical in ion probe work. At sufficiently low count rates, there is a significant probability that either the numerator or the denominator of the ratio will be zero, either of which violates the basic assumptions of the statistical analysis. To overcome this problem, the counts for ^{6}Li, ^{7}Li, ^{9}Be, ^{10}B, and ^{11}B were summed over the portion of the measurement where count rates were stable (integration times of 600 to 3000 s for a good run) to give the total counts for each isotope. Then the appropriate correction was applied for background count rate (0.015 to 0.028 cps, depending on run, compared with measured count rates of 0.1 to several cps for ^{10}B), and ^{7}Li/^{6}Li, ^{10}B/^{11}B, and ^{9}Be/^{11}B ratios were calculated. These ratios were then corrected for instrumental mass fractionation (50 to 60‰, depending on the run, favoring ^{7}Li; 40 to 50‰ favoring ^{10}B) and differential ion yield (0.37 to 0.44 with beryllium ionizing better). The appropriate counting-statistical errors and a 10% uncertainty in the sensitivity factor used to correct ion yield were propagated. Abundance standards were NBS 610 and NBS 612 glass (Pearce et al., 1997). These same glasses were also used as the lithium isotope standard with ^{7}Li/^{6}Li = 12.0394 determined by L.-H. Chan (unpublished) using thermal ionization as described in Chan (1987). Our boron isotope standard was BST–1 glass (450 ppm boron) prepared at ASU using SRM951 (^{10}B/^{11}B = 0.24718), and the boron isotope ratio was confirmed to be the same as that of SRM951 by bulk analysis (W. P. Leeman, personal communication).

2.2. Data Reduction

The ion yield of boron is a factor of $\sim$2.5 lower than that of beryllium. In combination with high Be/B ratios, this leads to a situation where the counting statistical uncertainty in ^{11}B makes a large contribution to the uncertainty of ^{9}Be/^{11}B, even though a 10% uncertainty in the sensitivity factor has been applied. The uncertainty on ^{10}B/^{11}B also has a large contribution from ^{11}B because we chose counting times that gave similar counting statistics for ^{10}B and ^{11}B. Thus, on a ^{9}Be/^{11}B vs. ^{10}B/^{11}B isochron plot, the data points have a large correlated component in the errors that does not contribute to the uncertainty in the calculated isochron. This phenomenon is well known in uranium-lead and lead-lead work, and software packages have been developed that calculate the appropriate errors for isochron plots (e.g., ISOPLOT by Ken Ludwig). For the beryllium-boron data, we have calculated error ellipses that separate the correlated and uncorrelated components and give the equivalent 2σ errors in ^{9}Be/^{11}B and ^{10}B/^{11}B. The difference that this calculation makes is typically 10–25%, but can be as large as 40%. The uncorrelated components were used to calculate the isochrons reported in this paper. No large correlated component is present in the aluminum-magnesium data, however, because ^{24}Mg (the denominator) is very well determined. Thus, the measured ratios were used to calculate aluminum-magnesium isochrons.

The isochron method works well to determine both the initial abundance ratio of the daughter isotope and the initial abundance of the parent isotope. It also handles small excesses of radiogenic isotopes well. However, isochron plots do not work as well when the underlying normal component is not well determined. A well-known example concerns the excess ^{26}Mg from decay of ^{26}Al in presolar Al_2O_3 and SiC grains, which contain essentially no magnesium. In these cases, it is often more reliable to calculate the initial abundance of the radiogenic ^{26}Mg directly by assuming that the underlying nonradiogenic magnesium has a normal ^{26}Mg/^{24}Mg ratio and then subtracting that compo-

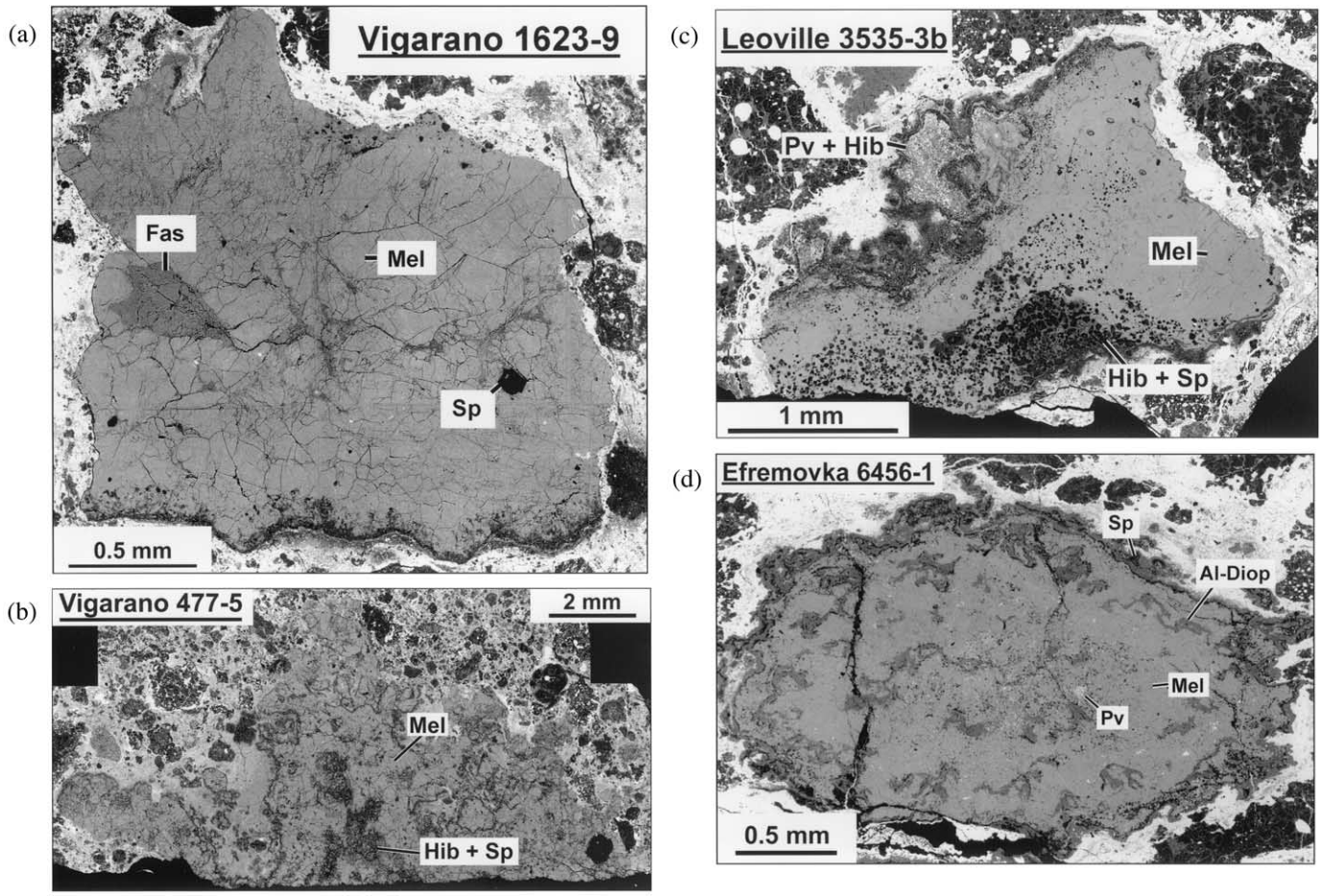

Fig. 1. Backscattered-electron images of four of the Type A CAIs measured in this study. (a) Vigarano 1623-9 is a CAI fragment consisting primarily of melilite (Mel) with minor fassaite (Fas) and rare spinel (Sp). A Wark-Lovering rim is present along the bottom edge of the CAI. (b) Vigarano 477-5 is a "fluffy" Type A CAI consisting of melilite nodules enclosing spinel and hibonite (Hib). (c) Leoville 3535-3b is a complex Type A inclusion consisting primarily of melilite with subordinate spinel, hibonite, and perovskite (Pv). (d) Efremovka 6456-1 is an elliptical Type A inclusion consisting primarily of melilite with subordinate spinel, hibonite, and perovskite. Aluminum-rich diopside (Al-Diop) occurs in the Wark-Lovering rim (with spinel) and as stringers within the CAI.

nent based on the measured abundance of the most abundant isotope (^{24}Mg; Huss et al., 1997). We have a similar situation in the most radiogenic boron measurements. The measured ^{10}B consists of the initial ^{10}B plus the radiogenic ^{10}B* from the decay of ^{10}Be. If ^{10}B* comprises a sufficiently high fraction of the total ^{10}B, its abundance can be calculated reliably by difference, if we know the composition of the underlying boron. The calculation is simply:

$$^{10}\mathrm{B}^{*} = {}^{10}\mathrm{B}_{\mathrm{meas}} - \left({}^{11}\mathrm{B} \times \left(\frac{^{10}\mathrm{B}}{^{11}\mathrm{B}} \right)_{\mathrm{initial}} \right)$$

Because the regressions give initial boron compositions close to normal terrestrial boron, we simply could have assumed that the non-radiogenic boron has a normal isotopic composition. However, because cosmic ray interactions could have affected the boron composition directly, we chose the more conservative option and used the intercept of the regression to define the normal component. The uncertainty in the intercept was propagated through the calculation. The initial ratios used were within 4% and 2.5σ of the terrestrial ratio. The ^{10}B* abundances were then divided by the measured ^{9}Be abundances, after appropriate corrections for sensitivity, to give the $(^{10}\mathrm{Be}/^{9}\mathrm{Be})_0$ ratios.

We carried out this calculation for the high ^{9}Be/^{11}B points of each inclusion (2 to 5 points per inclusion). The errors for ^{10}B* include the measurement error on ^{10}B, the measurement error on ^{11}B multiplied by the ^{10}B/^{11}B ratio, and the uncertainty in the ^{10}B/^{11}B ratio from the regression. For each inclusion, we then calculated the error-weighted mean of the estimates of $(^{10}\mathrm{Be}/^{9}\mathrm{Be})_0$ from the different points. The resulting ratios are in good agreement with those calculated from the isochrons, but the uncertainties are somewhat smaller. The main difference between the two methods of treating the data is that the difference calculation does not utilize points with low ^{9}Be/^{11}B ratios. In each of the isochron diagrams there are points with low to moderate ^{9}Be/^{11}B ratios that fall $\sim 2\sigma$ off of the regression line, which increases the uncertainty.

All isotopic data are reported with 2σ uncertainties

3. SAMPLE DESCRIPTIONS

Vigarano 1623-9 (Fig. 1a) is a rectangular Type A fragment, ~2 mm in size, consisting largely of melilite ($Åk_{2-66}$), with minor fassaite (10–12% TiO_2) and rare spinel. Much of the melilite is magnesium-rich relative to that in many other Type A inclusions; the most aluminum-rich melilite occurs exclusively within 10–20 μm of a Wark-Lovering rim sequence (Wark and Lovering, 1977) that is present only along one side

of the CAI. The inclusion is intensely fractured, but secondary alteration is minor and consists mostly of anorthite.

Vigarano 477-5 (Fig. 1b) is a ~1.2-cm "fluffy" Type A inclusion (MacPherson and Grossman, 1984), consisting of numerous individually rimmed nodules of densely crystalline aluminum-rich melilite ($Åk_{2-18}$) surrounding a large central core. The interior of the core is hibonite- and spinel-rich and is surrounded by more densely crystalline aluminum-rich melilite. Each melilite nodule encloses spinel grains and clusters of hibonite (also see MacPherson, 1985, called 477-2F1 therein; Davis et al., 1986, 1987). The many nodules are separated from one another and from the core by intervening meteorite matrix, but within each nodule and the core the only porosity is a result of fracturing. Melilite crystals within the nodules are reversely zoned, from magnesium-rich cores to aluminum-rich rims, similar to melilite crystals in other Fluffy Type A inclusions (MacPherson and Grossman, 1984). Minor amounts of secondary anorthite and aluminous diopside are present within the nodules, but sodium-rich secondary phases are absent.

Leoville 3535-3b (Fig. 1c) is a complex, irregularly shaped Type A inclusion, ~3 mm in maximum dimension, that was studied by MacPherson and Davis (1993). The main central portion of the inclusion consists of aluminous melilite ($Åk_{0-23}$) that is fractured but largely unaltered except for very minor anorthite. On one side of the inclusion, the melilite encloses dense swarms of spinel crystals and nodules and nodule fragments consisting of spinel + hibonite, and spinel + perovskite. Secondary minerals are nearly absent. The other side of the CAI is mostly free of the spinel-rich material, but is bordered by a locally very thick rim sequence that is notable for an extreme enrichment in perovskite and hibonite. Aluminum-magnesium isotopic data and trace element data were reported by MacPherson and Davis (1993).

Vigarano 477-4b is a ~5-mm sized elliptical Type B1 inclusion with a well-developed melilite-rich outer mantle. This CAI is distinctive because of the presence of a spinel-free island (melilite + pyroxene only; possibly a xenolith) within the spinel-rich main body of the inclusion. The inclusion contains melilite ($Åk_{10-74}$), fassaite, anorthite, spinel, numerous metal beads, and tiny crystals of hibonite near the rim. A minor volume of secondary sodium-rich alteration phases occurs mainly within the Wark-Lovering rim sequence (Caillet, 1990).

Efremovka 6456-1 (Fig. 1d) is an elliptical Type A inclusion, approximately 3 × 2 mm in size. Because the long axis of the CAI lies in the plane of intense flattening that characterizes the entire meteorite, it is likely that the original shape of the CAI was more nearly spherical. It consists mostly of fine-grained aluminous melilite ($Åk_{6-15}$) with subordinate tiny grains of spinel, perovskite, and hibonite. The perovskite and hibonite are concentrated towards the center of the CAI. Numerous stringers of banded anorthite + aluminous diopside occur throughout the inclusion and are structurally and mineralogically identical to layers within the somewhat convoluted Wark-Lovering rim that surrounds the entire inclusion.

Allende 3898 is a subrounded Type A CAI ~7 mm in maximum diameter, consisting mainly of melilite ($Åk_{1-45}$) with subordinate fassaite, spinel, rhönite, and perovskite. Descriptions of this CAI have been published previously (Teshima and Wasserburg, 1985; Podosek et al., 1991); the description by Podosek et al. (1991) is detailed and includes a photograph, and that work is also the source of the aluminum-magnesium data used herein. Allende 3898 is an important CAI because it was analyzed by Gray et al. (1973) for rubidium-strontium isotopic systematics (their sample D7) and was found to have the lowest initial $^{87}Sr/^{86}Sr$ ratio of any known solar system object. That value (0.69877) is a solar system chronological benchmark, designated by Gray et al. (1973) as "ALL". Effectively, it represents time zero in the history of the solar system and accordingly should help constrain the beryllium-boron isotopic systematics.

Axtell AXCAI 2771 is a 2 × 3 mm Type A inclusion (described in detail by Srinivasan et al., 2000; their Fig. 1) that consists predominantly of aluminum-rich melilite (mostly $Åk_{20-36}$, $Åk_{8-10}$ near the Wark-Lovering rim), spinel, perovskite, and sparse grains of hibonite. The inclusion is cut by veins of secondary (preterrestrial) alteration phases. Srinivasan et al. (2000) published isotopic data that show AXCAI 2771 to be a FUN inclusion: $(^{26}Al/^{27}Al)_0 < 1.1 \times 10^{-5}$, F_{Mg} ~15 to 18‰ amu^{-1}, $\delta^{50}Ti$ ~3‰.

4. ISOTOPIC RESULTS

Our data for magnesium and aluminum are presented in Table 1, and data for lithium, beryllium, and boron are given in Table 2. Isochron plots for aluminum-magnesium and beryllium-boron are presented in Figure 2. Magnesium-aluminum data for Allende 3898 and AXCAI 2771 plotted in Figure 2 are taken from Podosek et al. (1991) and Srinivasan et al. (2000), respectively.

All but one of the inclusions show well-defined correlations between $^{26}Mg/^{24}Mg$ and $^{27}Al/^{24}Mg$ that yield $(^{26}Al/^{27}Al)_0$ ratios close to the "canonical" value of 5×10^{-5}. The exception is the FUN inclusion AXCAI 2771, which gives an upper limit of $\sim 1 \times 10^{-5}$ (Srinivasan et al., 2000). Values for $(^{26}Al/^{27}Al)_0$ in the Type A CAIs range from $(3.7 \pm 1.8) \times 10^{-5}$ in Vig 1623-9 to $(5.1 \pm 1.3) \times 10^{-5}$ in Efremovka 6456. Within error, all of the isochrons are undisturbed, supporting the assumption that these inclusions have suffered little or no magnesium redistribution subsequent to their formation. The Type B1 inclusion Vigarano 477-4b has $(^{26}Al/^{27}Al)_0 = (4.6 \pm 1.4) \times 10^{-5}$ and also appears to be undisturbed.

All of the inclusions studied here show clearly resolved excesses of ^{10}B and good correlations between $^{10}B/^{11}B$ and $^{9}Be/^{11}B$, which together indicate in situ decay of ^{10}Be. The intercepts of the correlation lines give $(^{10}B/^{11}B)_0$ values that are within 4% of the normal terrestrial boron ratio. Those that differ outside of 2σ uncertainties lie both below and above the terrestrial ratio and thus provide no systematic indication of excess cosmogenic ^{10}B. Table 3 compares $(^{10}Be/^{9}Be)_0$ ratios calculated in the two ways noted earlier. The values in the column labeled "Regression method" come from error-weighted least-squares regressions of the data plotted in Figure 2, considering only the uncorrelated components of the errors as defined by the error ellipses (see Section 2.2). The column labeled "Difference method" gives $(^{10}Be/^{9}Be)_0$ ratios calculated directly from the measured ^{10}B and ^{9}Be and the intercept of the regressions, as described in Section 2.2. The estimates are in good agreement, with the values calculated by difference having somewhat smaller errors. The $(^{10}Be/^{9}Be)_0$ ratios for normal inclusions range from $\sim 0.48 \times 10^{-3}$ to $\sim 0.77 \times 10^{-3}$

Table 1. Al-Mg data for CAIs from CV3 chondrites

Phase	δ^{26}Mg	^{27}Al/^{24}Mg	Phase	δ^{26}Mg	^{27}Al/^{24}Mg	Phase	δ^{26}Mg	^{27}Al/^{24}Mg
Efremovka 6456-1 $(^{26}Al/^{27}Al)_0 = (5.1 \pm 1.3) \times 10^{-5}$								
Mel #1	9.2 ± 4.3	26.1 ± 1.3	Mel #6	6.7 ± 3.7	19.0 ± 1.0	Mel #11	7.1 ± 3.8	20.0 ± 1.0
Mel #2	10.9 ± 5.4	27.1 ± 1.4	Mel #7	3.0 ± 3.0	11.0 ± 0.6	Mel #12	10.5 ± 4.9	29.4 ± 1.5
Mel #3	11.5 ± 5.0	33.4 ± 1.7	Mel #8	7.4 ± 4.2	17.7 ± 0.9	Sp #1	0.5 ± 1.9	2.42 ± 0.12
Mel #4	9.8 ± 4.4	24.6 ± 1.3	Mel #9	5.5 ± 3.6	13.1 ± 0.7	Sp #2	2.1 ± 2.6	2.59 ± 0.13
Mel #5	7.8 ± 4.1	20.1 ± 1.1	Mel #10	7.7 ± 4.1	19.7 ± 1.0			
Vigarano 1623-9 $(^{26}Al/^{27}Al)_0 = (3.7 \pm 1.8) \times 10^{-5}$								
Mel #1	5.5 ± 5.3	16.8 ± 0.8	Mel #4	4.1 ± 3.9	15.5 ± 0.8	Sp #1	1.5 ± 1.9	2.38 ± 0.12
Mel #2	7.8 ± 4.6	27.2 ± 1.6	Mel #5	6.2 ± 4.4	21.0 ± 1.0	Sp #2	0.6 ± 2.1	2.38 ± 0.12
Mel #3	7.4 ± 4.7	25.9 ± 1.4						
Vigarano 477-4b $(^{26}Al/^{27}Al)_0 = (4.5 \pm 1.4) \times 10^{-5}$								
Mel #1	2.1 ± 1.8	6.1 ± 0.3	Mel #4	5.1 ± 2.6	15.6 ± 0.8	Sp #1	0.5 ± 1.8	2.41 ± 0.12
Mel #2	3.2 ± 2.3	8.5 ± 0.4	Mel #5	8.0 ± 2.4	24.1 ± 1.4	Sp #2	0.2 ± 2.3	2.05 ± 0.10
Mel #3	2.0 ± 2.3	8.9 ± 0.5	Mel #6	7.9 ± 4.0	28.8 ± 1.1			
Vigarano 477-5 $(^{26}Al/^{27}Al)_0 = (5.0 \pm 0.4) \times 10^{-5}$								
Mel #1	4.5 ± 1.5	13.5 ± 0.5	Mel #13	14.5 ± 1.2	36.5 ± 4.3	Sp #5	−0.0 ± 1.3	2.53 ± 0.04
Mel #2	22.0 ± 8.5	68 ± 16	Mel #14	2.8 ± 3.4	10.0 ± 0.6	Sp #6	−2.3 ± 3.7	2.53 ± 0.04
Mel #3	4.8 ± 4.2	15.8 ± 1.4	Mel #15	7.9 ± 7.5	18.8 ± 0.2	Sp #7	−1.1 ± 4.2	2.53 ± 0.04
Mel #4	10 ± 10	13.4 ± 0.3	Mel #16	10 ± 10	25.1 ± 0.2	Sp #8	4.6 ± 1.9	2.53 ± 0.04
Mel #5	23.8 ± 3.0	61 ± 16	Mel #17	14.3 ± 5.8	49.9 ± 2.0	Sp #9	2.1 ± 1.3	2.53 ± 0.04
Mel #6	23 ± 15	53.9 ± 3.3	Mel #3-48	61 ± 14	157 ± 14	Sp #10	4.7 ± 2.8	2.53 ± 0.04
Mel #7	14.7 ± 8.3	41 ± 13	Mel	4.6 ± 4.8	14.4 ± 1.2	Sp #11	3.9 ± 2.9	2.53 ± 0.04
Mel #8	11.6 ± 3.6	35.6 ± 4.3	Sp	0.1 ± 2.2	2.53 ± 0.04	Sp #12	2.8 ± 1.6	2.53 ± 0.04
Mel #9	24 ± 17	69.4 ± 1.1	Sp #1	−0.4 ± 1.8	2.53 ± 0.04	Sp #13	2.2 ± 3.9	2.53 ± 0.04
Mel #10	2.2 ± 9.3	17.8 ± 0.7	Sp #2	0.6 ± 2.3	2.53 ± 0.04	Sp #14	3.9 ± 1.2	2.53 ± 0.04
Mel #11	−1.4 ± 0.8	12.7 ± 1.6	Sp #3	−0.2 ± 1.6	2.53 ± 0.04			
Mel #12	14.2 ± 1.3	39.7 ± 0.5	Sp #4	3.6 ± 4.5	2.53 ± 0.04			
Leoville 3535-3b $(^{26}Al/^{27}Al)_0 = (4.6 \pm 0.8) \times 10^{-5}$								
Mel #1	7.6 ± 3.7	20.5 ± 1.0	Mel #8	12.1 ± 3.4	34.2 ± 1.7	Hib #3	13.3 ± 1.6	42.5 ± 0.4
Mel #2	5.4 ± 3.6	17.9 ± 0.9	Mel #9	6.0 ± 1.3	22.1 ± 0.1	Hib #4	15.5 ± 1.5	47.1 ± 1.2
Mel #3	12.0 ± 4.2	37.7 ± 1.9	Mel #10	20.9 ± 1.4	58.3 ± 0.4	Sp #1	1.2 ± 2.0	2.50 ± 0.13
Mel #4	9.3 ± 4.1	32.7 ± 1.6	Mel #11	29.5 ± 1.4	85.5 ± 0.3	Sp #2	0.5 ± 2.2	2.47 ± 0.12
Mel #5	11.8 ± 4.6	35.3 ± 1.8	Mel #12	22.5 ± 1.6	56.8 ± 0.2	Sp #3	1.0 ± 1.9	2.44 ± 0.12
Mel #6	12.2 ± 3.9	35.1 ± 1.8	Hib #1	12.8 ± 3.2	31.4 ± 1.6	Sp #1	2.4 ± 1.5	2.50 ± 0.04
Mel #7	9.7 ± 4.2	37.6 ± 1.9	Hib #2	3.5 ± 1.6	13.6 ± 0.3			

All errors are 2σ.
Mel = melilite; Hib = hibonite; Sp = spinel.

(Table 3). The $(^{10}Be/^{9}Be)_0$ ratio for the FUN inclusion, AXCAI 2771, falls at the low end of this range at $\sim 0.36 \times 10^{-3}$. Interestingly, the chronologic "benchmark" inclusion Allende 3898 also falls near the lower end of the range at $\sim 0.48 \times 10^{-3}$. These values are similar to those measured in CAIs from Allende and Efremovka, $\sim 0.45 \times 10^{-3}$ to $\sim 0.95 \times 10^{-3}$ (Sugiura et al., 2001; McKeegan et al., 2000; 2001).

5. DISCUSSION

5.1. ^{10}B Excesses: Decay of ^{10}Be, or Cosmogenic Boron?

Clear excesses of ^{10}B were found in all seven of the CAIs we measured. The correlations between ^{10}B/^{11}B vs. ^{9}Be/^{11}B suggest that these excesses resulted from the in situ decay of ^{10}Be after the CAIs had formed. However, another possible interpretation is that the correlations are two-component mixing lines connecting normal boron with boron produced by cosmic ray interactions. Before proceeding to discuss the data in terms of decay of ^{10}Be, therefore, it is critical to establish more rigorously that the observed arrays on ^{10}B/^{11}B vs. ^{9}Be/^{11}B plots really are isochrons. The cosmic ray interactions that could in theory produce the correlations in Figure 2 could not have occurred after the meteorite formed. The irradiations would have occurred either before or immediately after the CAI formed in an extremely particle-rich environment. Two tests can be applied that would indicate the ^{10}B excesses to be of cosmogenic rather than radiogenic origin: (1) the excesses should be independent of beryllium concentration; and (2) the observed values for ^{10}B/^{11}B must be within the range reasonable for production of ^{10}B by cosmic ray bombardment. Consider first beryllium content, using Efremovka 6456-1 and Leoville 3535-3b as examples. Varying mixtures of normal boron (^{10}B/^{11}B $\approx$ 0.2472) and cosmogenic boron (^{10}B/^{11}B $\approx$ 0.45) can, in principle, produce the correlations in Figure 2. However, if the excess ^{10}B is cosmogenic then the correlations in Figure 2 are actually ^{10}B/^{11}B vs. 1/^{11}B, and therefore the ^{9}Be content must be constant. Figure 3 shows that beryllium contents are far from constant and there are only weak correlations between ^{10}B/^{11}B and 1/^{11}B. Clearly, the correlations in Figure 2 are much stronger. Some of the other inclusions show reasonable correlations between ^{10}B/^{11}B and 1/^{11}B (e.g., Vig. 477-4b), but the correlations strengthen when ^{10}B/^{11}B is plotted against ^{9}Be/^{11}B. These observations provide strong support for in situ decay of ^{10}Be.

Turning now to ^{10}B/^{11}B ratios, cosmic ray interactions produce boron with ^{10}B/^{11}B ratios ranging between $\sim$0.3 and

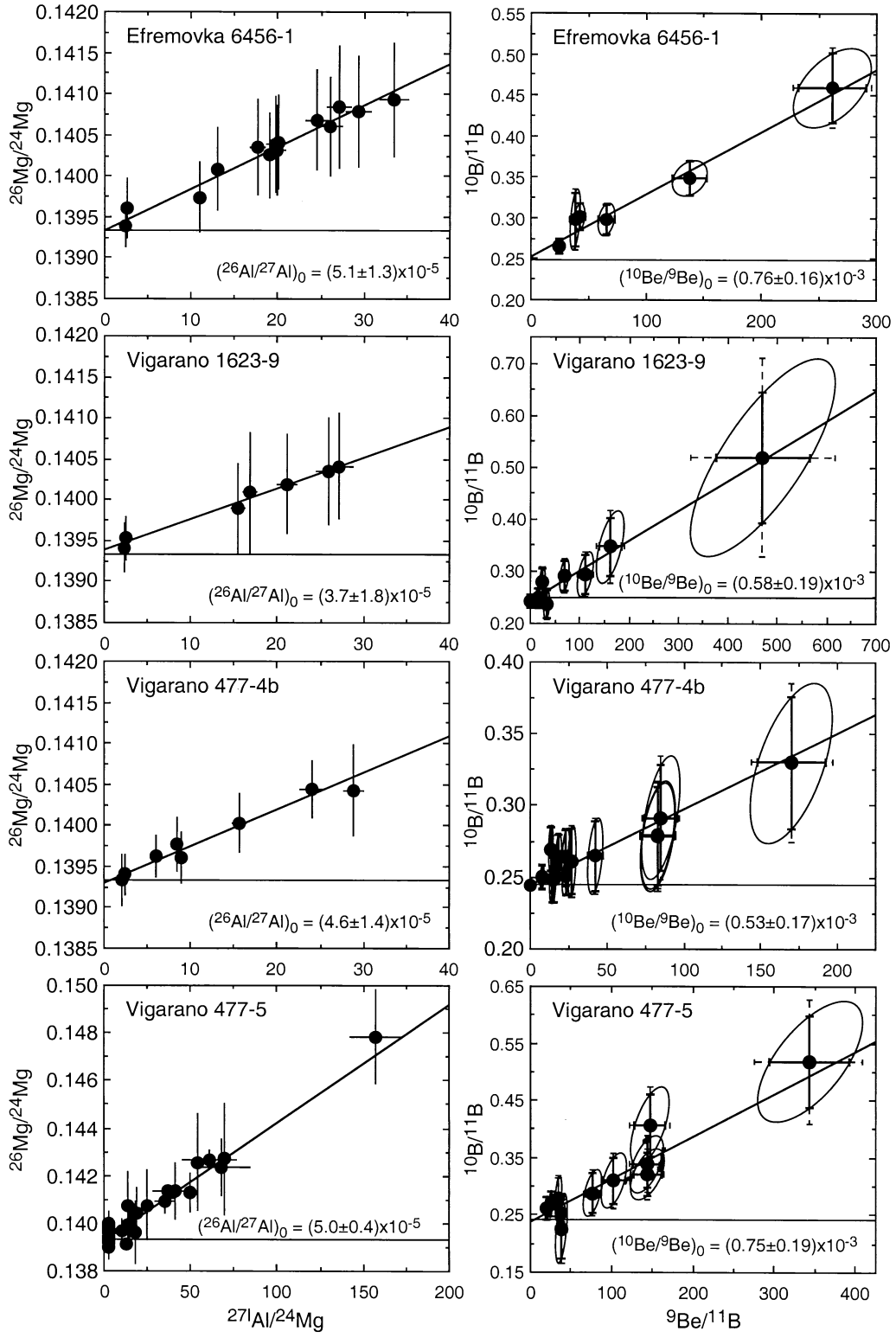

Fig. 2. Isochron diagrams for the seven inclusions measured in this study. The left panel for each inclusion shows the aluminum-magnesium data, including the $(^{26}Al/^{27}Al)_0$ ratio derived from the isochron. Error bars in the aluminum-magnesium diagrams are the 2σ statistical errors typically plotted for such analyses. The right panels show the beryllium-boron data, including the $(^{10}B/^{11}B)_0$ ratios derived from the isochrons. Errors analogous to those for aluminum-magnesium data are shown by the dashed error bars. However, because this error contains a large correlated component, we have also calculated the 88% confidence ellipse for the analysis, which separates the correlated and uncorrelated components. The corresponding 2σ errors on the ratios are shown as solid error bars. (Aluminum-magnesium data for Allende 3898 and AXCAI 2771 from Podosek et al., 1991, and Srinivasan et al., 2000, respectively.)

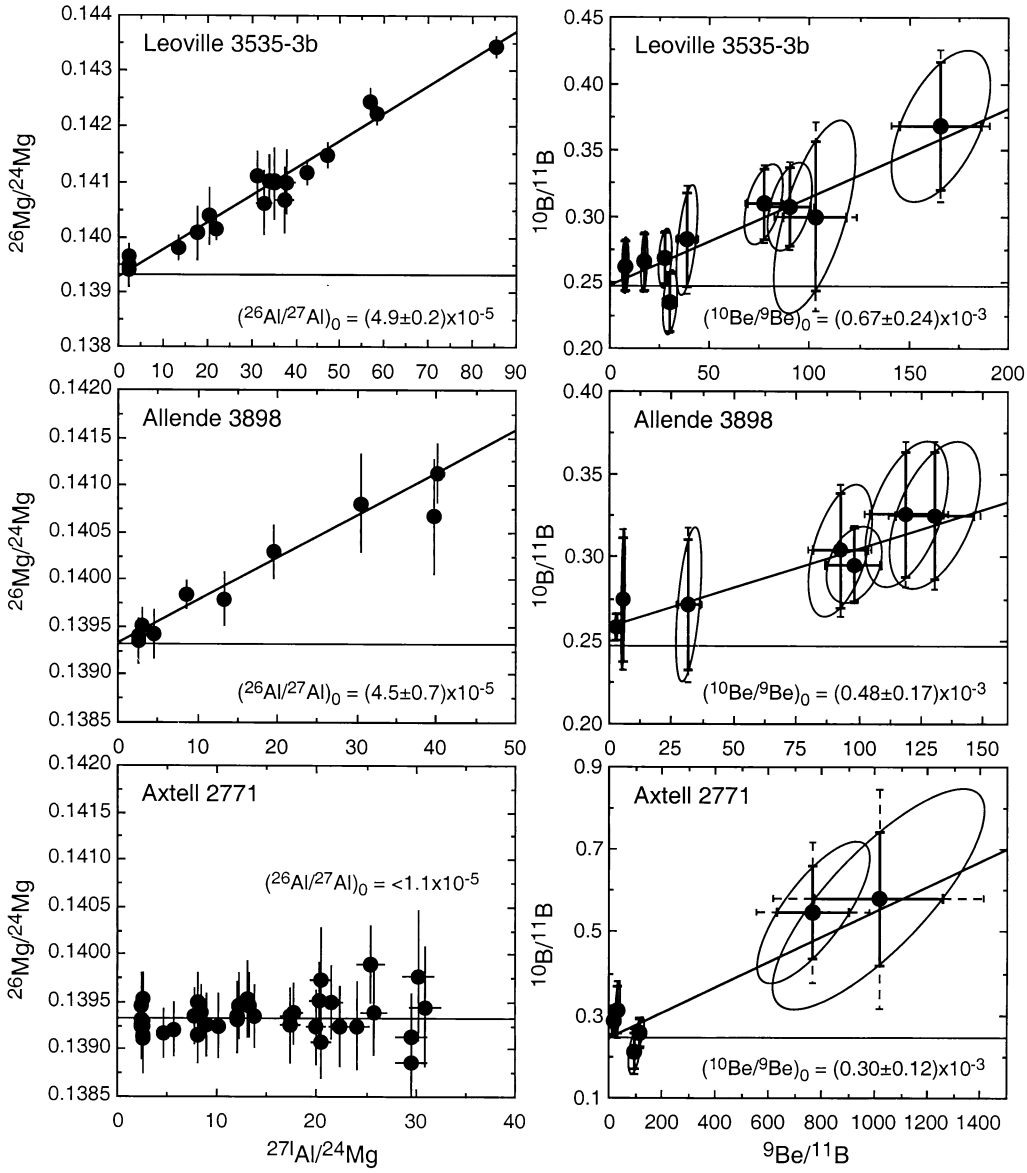

Fig 2. Continued

~0.6, depending on the energy spectrum and target element (Reeves, 1994; Reedy, 1989). A small amount of ^{10}Be is produced at the same time (~10% of the amount of ^{10}B; Reedy, 1989). However, for this ^{10}Be to have a significant effect, a chemical fractionation must enhance the ^{10}Be relative to ^{10}B. This would also enhance the total beryllium and lead back to the radiogenic scenario. Therefore, if the maximum observed ratios exceed those permissible by cosmic ray interaction models, then decay of ^{10}Be would be required to explain the observed boron isotopic compositions. In Vigarano 1623-9, Vigarano 477-5, and Axtell 2771, some of the measured ^{10}B/^{11}B ratios are at the upper end of the range calculated for cosmogenic boron (Table 2, Fig. 2). These ratios are not high enough to firmly exclude a cosmogenic source. However, for a mixing relationship between cosmogenic and normal boron to explain the data, the highest values measured in these inclusions would require virtually all of the boron to be cosmogenic and would imply no secondary introduction of normal boron into the inclusions or contamination by terrestrial boron. Because boron is present in alteration phases, and also is ubiquitous and hard to get rid of in the laboratory, the chances that we measured pure cosmogenic boron seem very low.

Production of cosmogenic boron will also result in coproduction of cosmogenic lithium. Production from oxygen-rich material would give similar amounts of boron and lithium, with lithium having ^{7}Li/^{6}Li $\approx$ 1.5, whereas about half as much lithium as boron would be produced from carbon-rich targets, with ^{7}Li/^{6}Li $\approx$ 1.8 (Reeves, 1994; Reedy, 1989). Mixing of this material with nonradiogenic material can appear to decouple the radiogenic components of the two elements. If mixing occurs before incorporation into a CAI, and lithium and boron are fractionated during incorporation, then the lithium and

Table 2. Lithium, beryllium, and boron data for CAIs from CV3 chondrites

	Li (ppm)	Be (ppm)	B (ppm)	$^{7}Li/^{6}Li^{a,b}$	$\Delta^{7}Li(‰)^{c}$	$^{10}B/^{11}B^{a,b,d}$	$\delta^{10}B(‰)^{b,d}$	$^{9}Be/^{11}B^{a,b,d}$
Efrem. 6456-1 $(^{10}Be/^{9}Be)_0^{e} = (0.76 \pm 0.16) \times 10^{-3}$					$(^{10}B/^{11}B)_0^{e} = 0.2522 \pm 0.0069$		$\Delta^{10}B_0^{f} = 20 \pm 28$	$\Delta^{7}Li_m^{g} = -52 \pm 12$
Mel #1	0.31 ± 0.04	30 ± 3	1.2 ± 0.2	10.4 ± 1.3	−137 ± 107	0.297 ± 0.039 (34)	202 ± 156 (139)	38.2 ± 5.2 (4.6)
Mel #2	0.54 ± 0.06	104 ± 10	2.4 ± 0.3	10.9 ± 0.9	−98 ± 71	0.298 ± 0.020 (19)	205 ± 82 (78)	65.9 ± 7.3 (7.0)
Mel #3	8.9 ± 0.9	125 ± 13	7.5 ± 0.8	11.6 ± 0.2	−34 ± 17	0.266 ± 0.009 (9)	76 ± 37 (37)	24.6 ± 2.5 (2.5)
Mel #4	0.25 ± 0.03	94 ± 9	3.3 ± 0.4	10.8 ± 0.6	−104 ± 49	0.302 ± 0.017 (16)	221 ± 67 (65)	42.0 ± 4.5 (4.4)
Mel #5	6.6 ± 0.7	161 ± 16	0.9 ± 0.1	11.3 ± 0.3	−59 ± 22	0.459 ± 0.051 (44)	856 ± 205 (178)	261 ± 34 (30)
Mel #6	1.34 ± 0.14	216 ± 22	2.3 ± 0.3	11.2 ± 0.5	−73 ± 41	0.348 ± 0.022 (21)	407 ± 90 (86)	137 ± 15 (14)
Vig. 1623-9 $(^{10}Be/^{9}Be)_0^{e} = (0.58 \pm 0.19) \times 10^{-3}$					$(^{10}B/^{11}B)_0^{e} = 0.2420 \pm 0.0084$		$\Delta^{10}B_0^{f} = -21 \pm 34$	$\Delta^{7}Li_m^{g} = -39 \pm 13$
Mel #1	10.7 ± 1.1	56 ± 6	3.4 ± 0.4	11.6 ± 0.4	−41 ± 31	0.279 ± 0.030 (27)	128 ± 122 (111)	24.2 ± 3.1 (2.8)
Mel #2	11.0 ± 1.1	57 ± 6	2.5 ± 0.3	11.5 ± 0.3	−46 ± 29	0.236 ± 0.030 (27)	−45 ± 119 (108)	33.8 ± 4.4 (4.0)
Mel #3	0.70 ± 0.07	28 ± 3	0.09 ± 0.03	12.0 ± 0.9	−6 ± 78	0.519 ± 0.192 (125)	1100 ± 774 (506)	470 ± 147 (96)
Mel #4	1.5 ± 0.2	35 ± 4	0.32 ± 0.06	11.4 ± 0.6	−56 ± 48	0.347 ± 0.070 (55)	402 ± 281 (224)	161 ± 29 (23)
Mel #5	4.4 ± 0.4	43 ± 4	0.57 ± 0.08	11.7 ± 0.3	−31 ± 27	0.294 ± 0.042 (36)	189 ± 169 (147)	110 ± 16 (14)
Mel #6	3.1 ± 0.3	31 ± 3	2.9 ± 0.3	11.5 ± 0.4	−45 ± 34	0.250 ± 0.020 (19)	9 ± 81 (77)	16.1 ± 1.9 (1.8)
Mel #7	1.7 ± 0.2	31 ± 3	0.67 ± 0.08	11.7 ± 0.4	−32 ± 33	0.290 ± 0.032 (29)	174 ± 130 (117)	69.2 ± 8.9 (8.0)
Pyx #1	0.41 ± 0.05	3.9 ± 0.4	9.5 ± 1.0	11.9 ± 1.5	−13 ± 128	0.243 ± 0.013 (13)	−17 ± 52 (51)	0.60 ± 0.07 (0.07)
Vig. 477-4b $(^{10}Be/^{9}Be)_0^{e} = (0.53 \pm 0.17) \times 10^{-3}$					$(^{10}B/^{11}B)_0^{e} = 0.2445 \pm 0.0014$		$\Delta^{10}B_0^{f} = -11 \pm 6$	$\Delta^{7}Li_m^{g} = -24 \pm 9$
Mel #1	1.0 ± 0.1	37 ± 4	2.3 ± 0.3	11.7 ± 0.7	−26 ± 54	0.264 ± 0.020 (19)	67 ± 82 (77)	23.6 ± 2.7 (2.5)
Mel #2	3.2 ± 0.3	45 ± 5	8.5 ± 0.9	11.7 ± 0.3	−27 ± 28	0.250 ± 0.008 (8)	11 ± 33 (33)	7.7 ± 0.8 (0.8)
Mel #3	1.5 ± 0.2	16 ± 2	1.5 ± 0.2	11.7 ± 0.4	−28 ± 31	0.249 ± 0.017 (16)	7 ± 67 (65)	15.7 ± 1.7 (1.6)
Mel #4	1.6 ± 0.2	13 ± 1	1.4 ± 0.2	12.0 ± 0.3	−7 ± 26	0.270 ± 0.016 (15)	91 ± 64 (62)	13.4 ± 1.4 (1.4)
Mel #5	0.31 ± 0.04	21 ± 2	0.37 ± 0.05	11.8 ± 0.7	−18 ± 56	0.279 ± 0.039 (34)	127 ± 156 (138)	83 ± 11 (10)
Mel #6	2.0 ± 0.2	25 ± 3	1.4 ± 0.2	11.7 ± 0.5	−32 ± 39	0.261 ± 0.025 (23)	56 ± 100 (93)	26.8 ± 3.2 (3.0)
Mel #7	5.8 ± 0.6	17 ± 2	1.38 ± 0.15	11.8 ± 0.3	−21 ± 27	0.264 ± 0.016 (16)	67 ± 66 (63)	18.5 ± 2.0 (1.9)
Mel #8	4.6 ± 0.5	14 ± 1	0.27 ± 0.04	11.7 ± 0.3	−27 ± 27	0.292 ± 0.042 (37)	180 ± 172 (150)	85 ± 12 (11)
Mel #9	2.5 ± 0.3	12 ± 1	1.21 ± 0.13	11.8 ± 0.4	−22 ± 37	0.248 ± 0.016 (16)	5 ± 66 (63)	14.9 ± 1.6 (1.6)
Mel #10	4.8 ± 0.5	16 ± 2	0.56 ± 0.07	11.6 ± 0.3	−41 ± 27	0.265 ± 0.027 (25)	73 ± 108 (99)	42.5 ± 5.2 (4.8)
Mel #11	6.1 ± 0.6	20 ± 2	1.27 ± 0.13	11.6 ± 0.3	−35 ± 26	0.250 ± 0.013 (12)	13 ± 51 (49)	23.4 ± 2.5 (2.4)
Mel #12	6.8 ± 0.7	20 ± 2	0.20 ± 0.03	11.9 ± 0.3	−12 ± 28	0.330 ± 0.055 (46)	336 ± 224 (187)	170 ± 27 (22)
Pyx #1	0.12 ± 0.01	1.26 ± 0.13	87 ± 9	11.8 ± 0.9	−18 ± 74	0.244 ± 0.002 (2)	−12 ± 6 (6)	0.021 ± 0.002 (2)
Vig. 477-5 $(^{10}Be/^{9}Be)_0^{e} = (0.75 \pm 0.19) \times 10^{-3}$					$(^{10}B/^{11}B)_0^{e} = 0.2372 \pm 0.0093$		$\Delta^{10}B_0^{f} = -40 \pm 38$	$\Delta^{7}Li_m^{g} = -50 \pm 15$
Mel #1	0.34 ± 0.04	25 ± 3	0.25 ± 0.04	10.5 ± 0.8	−125 ± 70	0.405 ± 0.073 (58)	638 ± 295 (223)	147 ± 25 (20)
Mel #2	0.45 ± 0.05	23 ± 2	0.34 ± 0.05	11.1 ± 0.8	−81 ± 64	0.309 ± 0.050 (42)	249 ± 200 (162)	103 ± 16 (13)
Mel #3	0.47 ± 0.05	20 ± 2	1.14 ± 0.13	11.2 ± 0.9	−64 ± 71	0.276 ± 0.030 (27)	115 ± 119 (87)	29.1 ± 3.6 (3.3)
Mel #4	0.76 ± 0.08	27 ± 3	2.0 ± 0.2	11.3 ± 0.8	−60 ± 65	0.264 ± 0.022 (20)	66 ± 89 (79)	19.8 ± 2.3 (2.2)
Mel #5	0.48 ± 0.05	19 ± 2	0.81 ± 0.11	10.9 ± 1.1	−98 ± 89	0.285 ± 0.044 (38)	154 ± 179 (139)	35.7 ± 5.3 (4.5)
Mel #6	0.57 ± 0.06	26 ± 3	0.54 ± 0.08	11.6 ± 0.6	−33 ± 52	0.288 ± 0.040 (35)	164 ± 163 (139)	76.7 ± 10.7 (9.4)
Mel #7	0.42 ± 0.04	29 ± 3	0.34 ± 0.05	11.6 ± 0.5	−39 ± 43	0.322 ± 0.044 (38)	302 ± 180 (139)	144 ± 20 (17)
Mel #8	1.31 ± 0.13	34 ± 3	1.37 ± 0.15	11.7 ± 0.4	−30 ± 33	0.255 ± 0.016 (16)	30 ± 66 (139)	37.6 ± 4.1 (4.0)
Mel #9	1.64 ± 0.18	2.9 ± 0.3	0.11 ± 0.02	11.1 ± 0.9	−79 ± 74	0.225 ± 0.061 (51)	−88 ± 247 (139)	38.9 ± 7.6 (6.5)
Mel #10	2.17 ± 0.22	19 ± 2	0.13 ± 0.02	11.6 ± 0.4	−37 ± 29	0.518 ± 0.110 (81)	1094 ± 445 (139)	342 ± 67 (49)
Mel #11	0.36 ± 0.04	28 ± 3	0.34 ± 0.05	11.2 ± 0.6	−67 ± 46	0.340 ± 0.049 (42)	375 ± 198 (139)	143 ± 21 (18)
Leo. 3535-3b $(^{10}Be/^{9}Be)_0^{e} = (0.67 \pm 0.24) \times 10^{-3}$					$(^{10}B/^{11}B)_0^{e} = 0.2476 \pm 0.0086$		$\Delta^{10}B_0^{f} = 2 \pm 35$	$\Delta^{7}Li_m^{g} = -63 \pm 11$
Mel #1	0.65 ± 0.07	10.1 ± 1.0	0.39 ± 0.06	11.4 ± 0.7	−50 ± 56	0.283 ± 0.041 (35)	142 ± 164 (118)	38.3 ± 5.5 (4.7)
Mel #2	1.7 ± 0.2	10.7 ± 1.1	0.94 ± 0.11	11.3 ± 0.4	−61 ± 32	0.266 ± 0.023 (21)	74 ± 93 (68)	16.8 ± 2.0 (1.8)
Mel #3	0.52 ± 0.05	7.6 ± 0.8	0.11 ± 0.02	11.9 ± 0.7	−13 ± 56	0.300 ± 0.071 (56)	214 ± 288 (201)	103 ± 20 (16)
Mel #4	0.74 ± 0.08	6.9 ± 0.7	1.4 ± 0.02	10.3 ± 0.5	−140 ± 44	0.263 ± 0.020 (19)	63 ± 81 (61)	7.5 ± 0.9 (0.8)
Mel #5	6.26 ± 0.63	11.7 ± 1.2	0.13 ± 0.02	11.5 ± 0.3	−45 ± 26	0.368 ± 0.057 (48)	490 ± 229 (157)	166 ± 25 (20)
Mel #6	2.50 ± 0.25	12.0 ± 1.2	0.22 ± 0.03	11.2 ± 0.3	−69 ± 28	0.308 ± 0.033 (30)	245 ± 135 (96)	90 ± 11 (10)
Mel #7	1.09 ± 0.11	10.2 ± 1.0	0.57 ± 0.06	11.2 ± 0.4	−70 ± 33	0.269 ± 0.020 (19)	87 ± 83 (61)	27.5 ± 3.1 (2.9)
Mel #8	11.1 ± 1.1	19.0 ± 1.9	0.40 ± 0.05	11.3 ± 0.3	−61 ± 26	0.310 ± 0.029 (26)	252 ± 117 (83)	77.4 ± 9.3 (8.6)
Mel #9	2.10 ± 0.21	11.5 ± 1.2	0.24 ± 0.04	11.4 ± 0.4	−56 ± 34	0.235 ± 0.024 (22)	−49 ± 96 (72)	29.9 ± 3.2 (3.3)
Allende 3898 $(^{10}Be/^{9}Be)_0^{e} = (0.48 \pm 0.17) \times 10^{-3}$					$(^{10}B/^{11}B)_0^{e} = 0.2576 \pm 0.0069$		$\Delta^{10}B_0^{f} = 41 \pm 29$	$\Delta^{7}Li_m^{g} = -46 \pm 10$
Mel #1	8.0 ± 0.8	46 ± 5	0.57 ± 0.08	11.4 ± 0.3	−56 ± 22	0.326 ± 0.044 (38)	318 ± 179 (154)	119 ± 17 (15)
Mel #2	2.9 ± 0.3	43 ± 4	0.68 ± 0.09	11.7 ± 0.4	−27 ± 35	0.304 ± 0.040 (35)	230 ± 163 (142)	93 ± 13 (11)
Mel #3	3.2 ± 0.3	43 ± 4	0.49 ± 0.07	11.5 ± 0.4	−43 ± 30	0.325 ± 0.045 (38)	315 ± 181 (155)	130 ± 18 (16)
Mel #4	3.9 ± 0.4	26 ± 3	15.6 ± 1.6	11.2 ± 0.4	−71 ± 31	0.258 ± 0.008 (8)	45 ± 33 (32)	2.5 ± 0.3 (3)
Mel #5	2.5 ± 0.3	12 ± 1	0.57 ± 0.09	11.9 ± 0.5	−8 ± 43	0.272 ± 0.047 (40)	99 ± 190 (160)	32 ± 5 (4)
Mel #6	7.8 ± 0.8	79 ± 8	1.20 ± 0.12	11.3 ± 0.2	−64 ± 19	0.296 ± 0.024 (22)	196 ± 95 (88)	98 ± 11 (11)
Sp #1	41.8 ± 4.2	6.8 ± 0.7	1.9 ± 0.3	11.8 ± 0.3	−23 ± 21	0.275 ± 0.043 (37)	110 ± 172 (149)	5.3 ± 0.8 (7)

Continued

Table 2. Continued

	Li (ppm)	Be (ppm)	B (ppm)	^{7}Li/^{6}Li[a,b]	Δ^{7}Li(‰)[c]	^{10}B/^{11}B[a,b,d]	δ^{10}B(‰)[b,d]	^{9}Be/^{11}B[a,b,d]
Axtell 2771	$(^{10}Be/^{9}Be)_0$[e] = (0.30 ± 0.12) × 10^{-3}			$(^{10}B/^{11}B)_0$[e] = 0.2469 ± 0.0188		$\Delta^{10}B_0$[f] = −2 ± 76		$\Delta^{7}Li_m$[g] = −48 ± 22
Mel #1	0.65 ± 0.07	12 ± 1	0.96 ± 0.13	12.2 ± 1.0	16 ± 85	0.288 ± 0.037 (33)	163 ± 150 (132)	18.9 ± 2.6 (2.3)
Mel #2	0.46 ± 0.05	8.8 ± 0.9	0.42 ± 0.08	9.9 ± 1.1	−171 ± 93	0.313 ± 0.070 (56)	267 ± 283 (225)	30.6 ± 5.9 (4.7)
Mel #3	0.44 ± 0.05	20 ± 2	0.04 ± 0.01	11.0 ± 0.6	−89 ± 53	0.547 ± 0.171 (111)	1212 ± 691 (450)	767 ± 210 (137)
Mel #4	0.14 ± 0.02	5.6 ± 0.6	0.08 ± 0.02	11.1 ± 1.3	−82 ± 107	0.213 ± 0.053 (43)	−140 ± 214 (175)	99 ± 20 (16)
Mel #5	2.6 ± 0.3	40 ± 4	0.50 ± 0.07	11.7 ± 0.4	−26 ± 33	0.259 ± 0.037 (32)	45 ± 148 (130)	117 ± 16 (14)
Mel #6	0.70 ± 0.07	17 ± 2	0.02 ± 0.01	11.5 ± 0.6	−44 ± 54	0.580 ± 0.267 (161)	1347 ± 1079 (652)	1014 ± 398 (241)

[a] ^{7}Li/^{6}Li and ^{10}B/^{11}B have been corrected for instrumental mass fractionation. ^{9}Be/^{11}B has been corrected for the differential ion yield.
[b] Errors include the contributions from the uncertainty in instrumental mass fractionation and, for ^{9}Be/^{11}B, sensitivity factor.
[c] Δ^{7}Li is calculated with respect to ^{7}Li/^{6}Li = 12.0394 (L.-H. Chan, unpublished).
[d] Numbers in parentheses are errors after the correlated component has been removed (see text).
[e] $(^{10}Be/^{9}Be)_0$ and $(^{10}B/^{11}B)_0$ values come from weighted linear regressions using the uncorrelated components of the errors.
[f] $\Delta^{10}B_0$ is calculated with respect to ^{10}B/^{11}B = 0.24718 (SRM951) [19].
[g] $\Delta^{7}Li_m$ is the weighted mean of the individual Δ^{7}Li values for the inclusion.
Mel = melilite; Hib = hibonite; Pyx = pyroxene; Sp = spinel.

boron effects will not be correlated. Alternatively, if the irradiation took place after the CAI formed, then the correlations could be maintained. Our data do not in fact show the inverse correlation between ^{10}B/^{11}B and ^{7}Li/^{6}Li that would be expected if in situ–produced cosmogenic boron and lithium were both present in the samples in high abundance. However, the relatively low precision of our data preclude entirely ruling out their presence.

Although we cannot rule out the presence of significant cosmogenic boron, the poor correlation between ^{10}B/^{11}B and 1/^{11}B and the high measured ^{10}B/^{11}B compared with expected ratios for cosmogenic boron point toward live ^{10}Be as the source of the anomalous boron and the cause of the correlations in Figure 2. For the remainder of the paper, we will assume that the correlations shown in Figure 2 do reflect the in situ decay of ^{10}Be in the CAIs.

5.2. ^{10}Be Isotope Systematics and Comparisons with ^{26}Al

Our data both confirm and expand on the initial results of McKeegan et al. (2000) and the subsequent data from Sugiura et al. (2001) and McKeegan et al. (2001). The data for all of our inclusions (except perhaps AXCAI 2771) fall on relatively tight isochrons that have 2σ uncertainties in their slopes of 25% to 35%. These isochrons suggest that the Be-B systems in these inclusions are undisturbed to any major degree. One of the challenges for future measurements is to obtain sufficiently precise isochrons to establish more conclusively whether or not the Be-B system has remained undisturbed.

Table 4 summarizes available data for all CAIs in which both Al-Mg and Be-B isotopes have been measured. The initial ^{10}Be/^{9}Be ratios among the non-FUN Type A CAIs in our study range from 0.48 × 10^{-3} to 0.77 × 10^{-3}. This is quite similar to the range reported for Type B CAIs from Efremovka and Allende as summarized in Table 4 (0.45 × 10^{-3} to 0.95 × 10^{-3}). Thus the currently available data give no evidence of a systematic difference in $(^{10}Be/^{9}Be)_0$ between the Type A and B inclusions. In contrast, whereas the Type A inclusions have aluminum-magnesium isochrons showing little evidence of disturbance, the isochrons in many of the measured Type B inclusions do appear to be disturbed (Sugiura et al., 2001; see also Podosek et al., 1991). The Be-B measurements generally are made in melilite in all CAI varieties. However, for Al-Mg measurements in Type B inclusions, the measured high-aluminum phase generally is anorthite, whereas in Type A inclusions it is melilite. This led Sugiura et al. (2001) to conclude that the Be-B system in melilite is more robust than the Al-Mg system in anorthite. It remains to be shown whether the Be-B system is more robust than the Al-Mg system when both are measured in melilite (or anorthite).

Figure 4 is a plot of $(^{10}Be/^{9}Be)_0$ vs. $(^{26}Al/^{27}Al)_0$ for the seven inclusions we studied. Superficial inspection suggests that the two isotopic systems are positively correlated. Three CAIs, Vigarano 477-5, Leoville 3535-3b, and Efremovka 6456-1, have the highest values for both $(^{10}Be/^{9}Be)_0$ and $(^{26}Al/^{27}Al)_0$. Vigarano 1623-9, Vigarano 477-4b, and Allende 3898 are roughly intermediate in both ratios, and AXCAI 2771 has

Table 3. Comparison of $(^{10}Be/^{9}Be)_0$ calculated by two different methods.

Inclusions	$(^{10}Be/^{9}Be)_0$ Regression method	$(^{10}Be/^{9}Be)_0$ Difference method	(# Pts)
Efremovka 6456-1	(0.76 ± 0.16) × 10^{-3}	(0.73 ± 0.11) × 10^{-3}	(3)
Vigarano 1623–9	(0.58 ± 0.19) × 10^{-3}	(0.53 ± 0.18) × 10^{-3}	(3)
Vigarano 477-4b	(0.53 ± 0.17) × 10^{-3}	(0.51 ± 0.11) × 10^{-3}	(4)
Vigarano 477-5	(0.75 ± 0.19) × 10^{-3}	(0.77 ± 0.12) × 10^{-3}	(5)
Leoville 3535-3b	(0.67 ± 0.24) × 10^{-3}	(0.73 ± 0.14) × 10^{-3}	(3)
Allende 3898	(0.48 ± 0.17) × 10^{-3}	(0.48 ± 0.13) × 10^{-3}	(4)
Axtell 2771	(0.30 ± 0.12) × 10^{-3}	(0.36 ± 0.09) × 10^{-3}	(2)

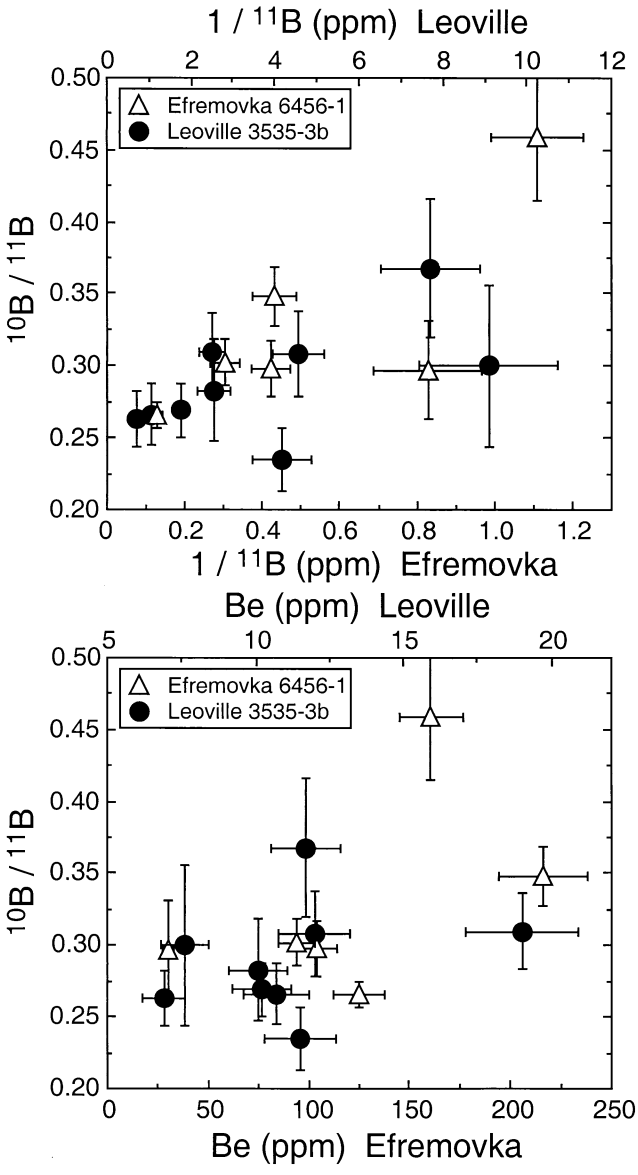

Fig. 3. The $^{10}B/^{11}B$ ratios are plotted against $1/^{11}B$ content and ppm beryllium for two inclusions to test the hypothesis that the boron ratios are due to cosmic ray interactions. The scales for Leoville 3535-3b are on the top of each panel, those for Efremovka 6456-1 are on the bottom. In the top panel, there is a hint of a correlation, but it is not as good as in Figure 2. The bottom panel shows that the beryllium content is not constant, but varies by factors of 2 to 3. These two data sets combine to form the good correlations in Figure 2, which strongly suggests that decay of ^{10}Be has produced the correlations.

the lowest values for both ratios. Interpreted in terms of free decay in a closed system, the difference in $(^{26}Al/^{27}Al)_0$ between the non-FUN CAIs with the highest ratios and the FUN CAI would correspond to a difference in formation time of at least 1.6 million years. This is roughly consistent with the time difference implied by $(^{10}Be/^{9}Be)_0$ for the same two CAIs, given the same assumptions, as shown by the upper line of concordant decay in Figure 4 (but see Section 5.5). However, this line is inconsistent with the data for three non-FUN CAIs. Considering just the "normal" inclusions, there appears to be a 50% variation in $(^{10}Be/^{9}Be)_0$ ratios but only a ~30% range in $(^{26}Al/^{27}Al)_0$. This is not what we would expect based on the half-lives of ^{10}Be and ^{26}Al (1.5 and 0.7 million years, respectively). The highest and lowest average values of $(^{10}Be/^{9}Be)_0$, each represented by three inclusions, are just resolved at the 2σ level. Figure 4 shows a second line of concordant decay, which assumes the lower $(^{10}Be/^{9}Be)_0$ ratio (0.5×10^{-3}). Neither curve is consistent with all of the data, although an intermediate curve ($\sim 0.6 \times 10^{-3}$) lies within 2.2σ of all of the data points. Higher precision data are clearly needed, but the existing data appear to us to be inconsistent with a single decay path, and this in turn suggests that the two isotopic systems are decoupled. This apparent decoupling implies that ^{10}Be and ^{26}Al were produced in different places or by different mechanisms.

5.3. Origin of the ^{10}Be and Relationships with Other Short-lived Nuclides

Lithium, beryllium, and boron are produced primarily through spallation reactions between galactic cosmic rays (GCR) and interstellar material. Inefficient production and burning in stellar interiors give very low lithium, beryllium, and boron abundances compared with other low-mass elements (Reeves, 1994). Therefore, one possibility is that the observed $(^{10}Be/^{9}Be)_0$ ratios in CAIs reflect the ambient concentration of ^{10}Be in the interstellar medium at the time the solar system was formed. McKeegan et al. (2000) calculated an upper limit on the steady-state $^{10}Be/^{9}Be$ in the contemporary interstellar medium of $\sim 8 \times 10^{-6}$, a factor of ~100 below the ratios inferred for the CAIs. We performed a different calculation using production rates (Reedy, 1989) for cosmic rays interacting with carbon and oxygen in small objects (simulating interstellar grains). Reedy's production rates were calculated from a geometric mean of four spectra for interstellar galactic cosmic rays (Reedy, 1987). The predictions for light isotopes, such as the isotopes of beryllium and boron, are relatively robust, but the estimates could be too low for low-energy reactions, such as production of neon from magnesium. If we assume a C/O ratio of ~0.42 and a solar system $^{9}Be/^{16}O$ ratio ($\sim 3 \times 10^{-8}$) (Anders and Grevesse, 1989), we calculate a steady-state interstellar $^{10}Be/^{9}Be$ ratio of $\sim 7 \times 10^{-5}$. This is somewhat higher than the ratio calculated by McKeegan et al. (2000) for the interstellar medium, but is still a factor of 6 to 10 below the observed abundance in CAIs. The difference between the two calculations primarily reflects the difference in the assumed relative amounts of ^{10}Be and ^{9}Be produced by cosmic rays ($^{10}Be/^{9}Be \approx 0.1$ in McKeegan et al., 2000 vs. ~0.25 to 0.45 in our calculation [Reedy, 1989]). Gounelle et al. (2001) did yet another calculation and found a steady-state $^{10}Be/^{9}Be$ ratio a factor of about 4 below the initial ratios observed in CAIs. All of these calculations require a cosmic ray flux 4.6 Ga ago that was greatly enhanced over that in the interstellar medium today to reproduce the observed $^{10}Be/^{9}Be$ ratios in CAIs.

Where might such an enhanced cosmic ray flux have existed? One possibility might be if the sun formed near a new O-star association in its parent molecular cloud. Molecular cloud complexes like the Orion complex spawn a variety of stars, from massive stars, which go supernova within a million years, to low-mass stars similar to our sun (Goudis, 1982). Star-forming regions have several mechanisms by which cos-

Table 4. Comparison of $(^{10}Be/^{9}Be)_0$ and $(^{26}Al/^{27}Al)_0$ in Type A and Type B CAIs.

Inclusion	Type	$(^{10}Be/^{9}Be)_0$ ($\times 10^{-3}$)	$(^{26}Al/^{27}Al)_0$ ($\times 10^{-5}$)	Source
Efremovka 6456-1	A	0.73 ± 0.11[a]	5.1 ± 1.3	This study
Vigarano 1623-9	A	0.53 ± 0.18[a]	3.7 ± 1.8	This study
Vigarano 477-5	A	0.77 ± 0.12[a]	5.0 ± 0.4	This study
Leoville 3535-3b	A	0.73 ± 0.14[a]	4.9 ± 0.2	This study
Allende 3898	A	0.48 ± 0.13[a]	4.5 ± 0.7	This study, Podosek et al. (1991)
Axtell CAI2771	A (FUN)	0.36 ± 0.09[a]	<1.1	This study, Srinivasan et al. (2000)
Efremovka E-44	B	0.84 ± 0.19	6.7 ± 2.2 (mel) 4.6 ± 1.1 (an)	McKeegan et al. (2001)
		0.76 ± 0.19	disturbed	Sugiura et al. (2001)
Efremovka E-48	A/B	0.81 ± 0.31	<0.009	Sugiura et al. (2001)
Efremovka E-54	B	0.45 ± 0.11	not measured	McKeegan et al. (2001)
Efremovka E69	B	0.61 ± 0.19	disturbed	Sugiura et al. (2001)
Efremovka E107	B	0.65 ± 0.21	not measured	McKeegan et al. (2001)
Efremovka E-38	B1	0.60 ± 0.12	disturbed	Sugiura et al. (2001)
Allende 477-4b	B1	0.51 ± 0.11	4.6 ± 1.4	This study
Allende 3529-Z	B	0.76 ± 0.26	4.0 ± 0.1[b]	Podosek et al. (1991)
Allende 001	B	0.53 ± 0.24	disturbed	Sugiura et al. (2001)
Allende 002	B	0.69 ± 0.10	<0.27	Sugiura et al. (2001)
Allende 3529-41	B	0.95 ± 0.19	4.1 ± 1.2	Podosek et al. (1991)

[a] Initial ratios calculated by difference methods (see text).
[b] Mildly disturbed.
mel = melilite; an = anorthite.

mic ray interactions could be enhanced (Clayton and Jin, 1995). These include complete stopping of galactic cosmic rays in dense cloud cores, and local acceleration of particles to cosmic ray velocities in the winds of nearby very massive stars or supernova explosions in the O-star associations. At energies above 10 MeV per nucleon, ^{9}Be and ^{10}Be are produced efficiently in average molecular-cloud material by cosmic rays with a composition typical of galactic cosmic rays ($^{10}Be/^{9}Be \approx 0.25$ to 0.5; Reedy, 1989). Interactions at these energies sufficient to produce the $(^{10}Be/^{9}Be)_0$ ratios inferred for CAIs would produce only a small fraction of the corresponding inferred initial ^{26}Al abundances. Anomalous lower-energy $^{16}O^{+}$-enriched cosmic rays can produce ^{26}Al more efficiently, but special conditions would be required to produce both ^{10}Be and ^{26}Al in their observed proportions (Clayton and Jin, 1995). Efficient production of ^{26}Al in the Orion molecular cloud complex was suggested by a report from the COMPTEL team (Bloemen et al., 1994) of a high level of nuclear excitation of ^{12}C (4.43 MeV) and ^{16}O (6.13 MeV) (Clayton and Jin, 1995). However, the initial reports of significant emission in these lines have turned out to be spurious (Bloemen et al., 1999), removing any direct evidence for a high rate of production of ^{26}Al by cosmic ray interactions in molecular clouds. Thus, a sufficiently intense irradiation environment in the sun's parent molecular cloud could have produced the observed ^{10}Be excesses in CAIs, but this environment is not likely to have produced much ^{26}Al.

Cameron (2001) proposed a very different model in which all of the short-lived radionuclides could have been produced from a single supernova that triggered the formation of the solar system. In this model, the supernova ejecta would generate significant quantities of ^{10}Be through spallation reactions as nuclei accelerated by the supernova explosion impact atoms in the ambient interstellar gas, while nuclides such as ^{26}Al, ^{41}Ca, ^{53}Mn, and ^{60}Fe would be produced in the supernova itself. This model would marginally decouple the production of ^{10}Be and ^{26}Al, but would supply both radionuclides with a single mechanism. Models of this type for production of short-lived radionuclides in the sun's parent molecular cloud need further study.

Another possibility is that ^{10}Be was produced by an enhanced particle flux from the early sun itself (Lee et al., 1998; Gounelle et al., 2001). Reasonable fluxes will produce the observed $(^{10}Be/^{9}Be)_0$ ratios for CAIs (McKeegan et al., 2000). However, some current models attempt to generate all the observed short-lived radionuclides (except perhaps ^{60}Fe) by irradiation near the protosun (Lee et al., 1998; Gounelle et al., 2001), and these require special conditions to be successful. The irradiation parameters necessary to produce the $(^{10}Be/^{9}Be)_0$ ratios inferred for CAIs can be made consistent with inferred ^{41}Ca and ^{53}Mn abundances (McKeegan et al., 2000), but it is extremely difficult to account for the inferred $(^{26}Al/^{27}Al)_0$ ratios in the same way. This is because ^{27}Al is $\sim 10^5$ times more abundant than ^{9}Be in average cosmic material (Anders and Grevesse, 1989). Thus, to produce the observed ratios from cosmic material, assuming no initial abundances of ^{10}Be and ^{26}Al, ^{26}Al must be produced $\sim 5 \times 10^3$ times more efficiently than ^{10}Be, ignoring the shorter half-life of ^{26}Al ($10^5 \times 5 \times 10^{-5}$ vs. $1 \times 1 \times 10^{-3}$). Adding in the steady-state galactic abundances of ^{10}Be and ^{26}Al ($^{10}Be/^{9}Be = 8 \times 10^{-6}$ [McKeegan et al., 2000] to $\sim 7 \times 10^{-5}$ [see above] and $^{26}Al/^{27}Al \approx 5 \times 10^{-7}$ [Clayton et al., 1993]) decreases the required relative production rate by only a few percent. Production of ^{26}Al by cosmic ray protons with a typical energy distribution is only $\sim$25 times more efficient than ^{10}Be production through irradiation of magnesium, aluminum, silicon, calcium, iron, etc. (Reedy, 1989). Conversely, ^{10}Be is efficiently produced from oxygen, a major constituent of nearly all solids, whereas ^{26}Al cannot be made from oxygen. Thus, proton irradiation of any roughly cosmic composition cannot generate $\sim 5 \times 10^3$ times more ^{26}Al than ^{10}Be. In fact, proton irradiation of average

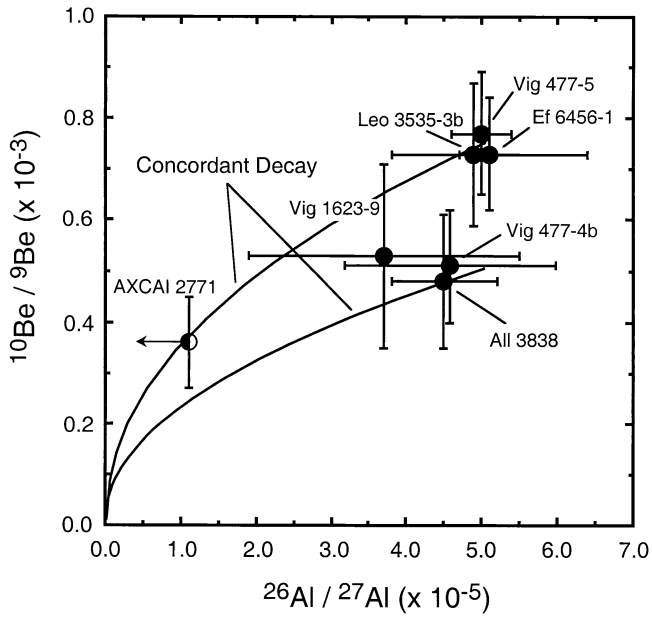

Fig. 4. Initial ^{10}Be/^{9}Be vs. initial ^{26}Al/^{27}Al for the CAIs measured in this study. The ^{26}Al/^{27}Al for the FUN inclusion, AXCAI 2771, is an upper limit, and all ^{10}B/^{11}B ratios were calculated by the difference method (Table 3). Notice that ^{10}Be/^{9}Be ratios vary by a factor of ~2, while the ^{26}Al/^{27}Al ratios for five of six non-FUN inclusions are between 4.5×10^{-5} and 5×10^{-5}. The lines labeled "Concordant Decay" describe two paths taken by material with different initial ^{10}Be/^{9}Be ratios (0.75×10^{-3} [upper], and 0.5×10^{-3} [lower]) and ^{26}Al/^{27}Al = 5×10^{-5} in a closed system. Among non-FUN inclusions, the highest and lowest ^{10}B/^{11}B ratios are resolvably different, whereas their initial ^{26}Al/^{27}Al ratios cannot be resolved. These data imply that ^{10}Be and ^{26}Al have different sources.

cosmic material cannot have generated the ^{26}Al found in CAIs, because the ^{26}Al is not accompanied by sufficient ^{10}Be.

One proposal to bring ^{26}Al production into line with those of other nuclides is for the irradiation to happen in impulsive flares (Lee et al., 1998), which in today's Sun are enriched in ^{3}He cosmic rays by up to 1000× relative to the solar ^{3}He/H ratio (Reames et al., 1997; Mandzhavidze et al., 1999). These ^{3}He cosmic rays are of low energy and have a steep energy spectrum (<20 MeV, with most of the energy below 1 MeV) (Bloemen et al., 1994). The astrophysical site proposed for this irradiation is the magnetic-reconnection ring surrounding the young active sun coupled with an X-wind (Shu et al., 1996) to get irradiated material out to the asteroid belt to be incorporated into meteorites (Lee et al., 1998; Shu et al., 2001). The key to this proposal is that at these low energies, proton reactions, which are most efficient at energies above 100 MeV, are effectively suppressed, while ^{3}He reactions proceed relatively efficiently. With the increased abundance of ^{3}He relative to protons in the accelerated particles, and with the much higher efficiency of ^{3}He reactions that produce ^{26}Al compared with other reactions, it becomes possible to generate enough ^{26}Al to explain the $(^{26}\text{Al}/^{27}\text{Al})_0$ ratios in CAIs. Using impulsive flares in the reconnection ring, Lee et al. (1998) were able to approximately match observed abundances of ^{41}Ca and ^{53}Mn by proton reactions and ^{26}Al by ^{3}He reactions (as well as make predictions for ^{138}La, and ^{50}V). However, because ^{41}Ca (and ^{50}V) are also produced by ^{3}He reactions along with ^{26}Al, the net result is a huge overproduction of ^{41}Ca relative to what is actually observed in CAIs. Lee and coworkers proposed three solutions to the overproduction of ^{41}Ca: (1) a layer structure for CAI precursors with an outer layer free of calcium; (2) chemical reequilibration of the CAIs such that potassium has been introduced and masks the true size of the ^{41}Ca anomaly; and (3) "if gradual flares rather than impulsive flares provide the dominant irradiation mechanism, ^{3}He reactions may not contribute to the production of radionuclides. The ^{41}Ca, ^{53}Mn, and ^{138}La can be made at their inferred CAI levels by proton and alpha irradiation within the solar system, but ^{26}Al would need to come from a galactic source" (Lee et al., 1998). These authors went on to show that ^{60}Fe cannot be produced by irradiation of any kind because it is too neutron-rich, and that known mechanisms fail by two orders of magnitude to produce even the low level of ^{60}Fe inferred for the early solar system from measurements in eucrites (Shukolyukov and Lugmair, 1993).

Gounelle et al. (2001) evaluated quantitatively the suggestion (#1 in the previous paragraph) that bombardment of mantled CAI precursors by ^{3}He might be able to explain the short-lived radionuclides in the CAIs. They adopted a two-component model of proto-CAIs in which cores with elemental abundances of Type B1 CAIs are mantled by less refractory (Ca-poor) material. For the irradiation site, they propose flares in the magnetic reconnection ring surrounding the protosun, in which the cosmic ray spectrum is believed to be similar to that in impulsive flares (Shu et al., 2001). The composition of the accelerated cosmic rays was chosen to have ^{3}He/H = 0.3. Under these conditions, Gounelle et al. (2001) were able to match the abundances of ^{10}Be, ^{26}Al, and ^{41}Ca, while producing about half of the inferred ^{53}Mn. However, to generate this match, they had to choose parameters that are at the extreme limits of observations. First, the irradiation must occur exclusively at low energies because the production rate of ^{10}Be rises rapidly at higher energies (Lee et al., 1998). Later exposure to higher-energy protons is also a problem. Second, the ^{4}He/H and ^{3}He/^{4}He ratios in impulsive flares are both enhanced, but ^{3}He/H ratios that exceed 0.1 appear to be extremely rare (Reames et al., 1997; Mandzhavidze et al., 1999). Thus, Gounelle et al. require cosmic rays with a composition rarely if ever observed in modern impulsive flares. Finally, to keep from overproducing ^{41}Ca, they require the calcium-poor mantle on the CAI precursors. Some CAIs have been found within chondrules (Bischoff and Keil, 1984; Krot et al., 1999; Russell and Kearsley, 1999), and accretionary rims are common on CAIs in CV chondrites (MacPherson et al., 1985). But in these known examples, the calcium-poor mantles are very irregular in thickness. They do not uniformly blanket entire CAI surfaces. It seems unlikely to us that a model requiring so many parameters at the extremes of plausibility can accurately describe the origin of the short-lived radionuclides in the early solar system. On the other hand, target chemistry can make a huge difference in the relative production rates of different nuclides and it is hard to rule out that irradiation of unusual targets has played some role in the production or short-lived radionuclides in chondritic material.

Although it obviously is tempting to try to explain the abundances of all the observed short-lived radionuclides by a single production mechanism, as in the models described

above, we argue that the evidence given in this paper (e.g., Fig. 4) for decoupling of the aluminum-magnesium and beryllium-boron isotopic systems makes such attempts misguided. It is generally agreed that ^{60}Fe cannot have been made by cosmic ray bombardment, and the bulk of the evidence suggests that the ^{26}Al cannot have been so made either. Certainly, some ^{10}Be, ^{41}Ca, and ^{53}Mn were produced through irradiation by cosmic ray protons and alpha particles having a normal energy distribution. The question is how much. Calculations assuming plausible cosmic ray fluxes suggest that only a few percent of the ^{26}Al, as much as half of the ^{53}Mn, and perhaps most of the ^{41}Ca needed to explain observations in CAIs can be produced by normal cosmic ray protons and alpha particles (Lee et al., 1998). The remaining >90% of the ^{26}Al, all of the ^{60}Fe, and the rest of the ^{53}Mn were most likely derived from one or more stellar sources and were imported into the solar system via presolar dust.

5.4. Implications for Chronometry and Nebular Heterogeneity

Short-lived nuclides are potential high-resolution chronometers of early solar system events, to the extent that it can be shown that they were widely distributed and isotopically homogeneous in the early solar system. But ^{10}Be may not satisfy these required conditions. Depending on the details of the irradiation mechanism, objects with high initial $(^{10}Be/^{9}Be)_0$ ratios could have been produced over an extended period of time, or objects with a range of $(^{10}Be/^{9}Be)_0$ ratios could have been produced at approximately the same time. In either case, the resulting ratios would contain little chronological information. The $(^{10}Be/^{9}Be)_0$ ratios in non-FUN Type A CAIs exhibit rather more variability (just resolved at 2σ precision) than corresponding $(^{26}Al/^{27}Al)_0$ ratios (Fig. 4), contrary to expectations based on the shorter half-life of ^{26}Al (0.7 Ma vs. 1.5 Ma for ^{10}Be). This observation implies that the CAI-forming region was not homogeneous with respect to ^{10}Be. Type B CAIs show a similar variability in $(^{10}Be/^{9}Be)_0$ to Type A CAIs, but their aluminum-magnesium systematics are often disturbed (Table 4). If the beryllium-boron system in Type Bs is not as easily reset as the aluminum-magnesium system, the variation in $(^{10}Be/^{9}Be)_0$ ratios in Type Bs may also be a primary signature, in which case Type A and B CAIs both record the $(^{10}Be/^{9}Be)_0$ variability of the early solar system. Certainly the $(^{10}Be/^{9}Be)_0$ variability in non-FUN Type A and Type B inclusions with $(^{26}Al/^{27}Al)_0 \approx 5 \times 10^{-5}$ cannot be interpreted in terms formation from a homogenous (in ^{10}Be) reservoir over a 1.5 million year time period. We conclude from the variability in the data that ^{10}Be may not be a good chronometer. Conversely, the relative consistency of $(^{26}Al/^{27}Al)_0$ ratios among the normal CAIs that have not been isotopically disturbed suggests that the aluminum-magnesium system is likely to be a better chronometer because it points to a nebula more nearly homogenous in ^{26}Al than in ^{10}Be (see also MacPherson et al., 1995; Huss et al., 2001).

5.5. Implications for the Origin of FUN Inclusions

The Type A FUN inclusion, AXCAI 2771, has a $(^{10}Be/^{9}Be)_0$ ratio ($\sim 0.36 \times 10^{-3}$) that is at the low end of the range exhibited by the non-FUN inclusions we analyzed. In contrast, AXCAI 2771 has an upper limit for $(^{26}Al/^{27}Al)_0$ that is far below the resolved ratios measured for the other Type A inclusions (Figs. 1 and 4). FUN CAIs are defined in part by having isotopic anomalies in essentially all elements, unlike non-FUN CAIs, so the lack of a significant difference in $(^{10}Be/^{9}Be)_0$ stands out. We noted above that, considering only the Al-Mg and Be-B systems, the data are consistent with AXCAI 2771 having formed from the same material reservoir as, but ~2 Ma later than, the inclusions with the highest $(^{10}Be/^{9}Be)_0$ ratios. However, the range of $(^{10}Be/^{9}Be)_0$ ratios for the other (non-FUN) CAIs appears (within the precision of our data) to make this or any other chronological interpretation unsupportable. Moreover, AXCAI 2771 (like other FUN inclusions) possesses intrinsic isotopic anomalies (e.g., Ti; Srinivasan et al., 2000) that are difficult to reconcile with its forming 2 Ma *later* than non-FUN CAIs; in this sense AXCAI 2771 is a prime example of decoupling between ^{26}Al and ^{10}Be because its lack of ^{26}Al probably is not the result of chronology. Even though ^{10}Be was apparently incorporated into AXCAI 2771 from the same source, by the same mechanism, and possibly even in the same place that it was incorporated into normal inclusions, the remaining bulk of AXCAI 2771 apparently represents a very different isotopic reservoir.

6. CONCLUSIONS

We have found clear evidence of live ^{10}Be in five normal Type A CAIs, one normal Type B CAI, and one FUN Type A CAI. The $(^{10}Be/^{9}Be)_0$ ratios range from $\sim 0.36 \times 10^{-3}$ to $\sim 0.77 \times 10^{-3}$ and are similar to those found in Type B inclusions by previous workers. The $(^{10}Be/^{9}Be)_0$ ratios appear not to correlate with $(^{26}Al/^{27}Al)_0$. Our examination of the production mechanisms for ^{10}Be and other radionuclides confirms the conclusions of previous workers that ^{10}Be was almost certainly produced by particle irradiation, probably but not necessarily within the solar system. Irradiation also could have contributed significantly to the inferred inventories of ^{41}Ca and ^{53}Mn. However, the existing body of evidence suggests to us that all of the ^{60}Fe, some ^{53}Mn, and most of the ^{26}Al were probably produced in stars and were brought into the solar system. It remains to be determined what role, if any, irradiation may have played in producing inferred inventories of this last group of short-lived radionuclides.

Acknowledgments—Our sincere thanks go to Frank Podosek and Shogo Tachibana for helpful and detailed discussion of error analysis and to Ken Ludwig for making his program, ISOPLOT, available to us. Lengthy discussions with Bob Reedy significantly improved our understanding of cosmogenic nuclide production, and his generous unofficial review resulted in substantial improvement to the paper. Thoughtful reviews by Peter Hoppe, François Robert, Associate Editor Uli Ott, and an anonymous reviewer are gratefully acknowledged. This work was supported by NASA grants NAG5-7396 (G.J.M.), NAG5-8158 (G.R.H.), and NAG5-9510 (A.M.D.).

Associate editor: U. Ott

REFERENCES

Anders E. and Grevesse N. (1989) Abundances of the elements: Meteoritic and solar. *Geochim. Cosmochim. Acta* **53,** 197–214.

Bischoff A. and Keil K. (1984) Al-rich objects in ordinary chondrites: Related origin of carbonaceous and ordinary chondrites and their constituents. *Geochim. Cosmochim. Acta* **48,** 693–709.

Bloemen H., Wijands R., Bennett K., Diehl R., Hermsen W., Lichti G., Morris D., Ryan J., Schönfelder V., Strong A. W., Swanenburg B. N., de Vries C., and Winkler C. (1994) COMPTEL observations of the Orion complex: Evidence for cosmic-ray induced gamma-ray lines. *Astron. Astrophys* **281,** L5–L8.

Bloemen H., Morris D., Knödelseder J., Bennet K., Diehl R., Hermsen W., Lichti G., van der Muelen R. D., Oberlack U., Ryan J., Schönfelder V., Strong A. W., de Vries C., and Winkler C. (1999) The revised Comptel Orion results. *Astrophys. J.* **521,** L137–L140.

Caillet C. (1990) Mineralogie des meteorites: 1–Description d'une nouvelle chondrite de Type H3 trouvee a Sainte Rose, La Reunion. (France). 2–L'inclusion alumino-calcique 477B de la chondrite carbonee Vigarano: Etude de quelques 'fremlinge'. These de doctorat, L'Universite Pierre et Marie Curie. 240 pp.

Cameron A. G. W. (1993) Nucleosynthesis and star formation. In *Protostars and Planets III* (eds. E. H. Levy and J. I. Lunine). Univ. of Arizona Press, Tucson, pp. 47–73.

Cameron A. G. W. (2001). Extinct radioactivities and the r-process jet. *Lunar Planet. Sci. XXXII.* Lunar Planet. Inst., Houston. #1035 (abstr.).

Cameron A. G. W., Höflich P., Myers P. C., and Clayton D. D. (1995) Massive supernovae, Orion gamma rays, and the formation of the solar system. *Astrophys. J.* **447,** L53–L57.

Catanzaro E. J., Murphy T. J., Garner E. L., and Shields W. R. (1966) Absolute isotopic abundance ratios and atomic weights of magnesium. *J. Res NBS* **70A,** 453–458.

Chan L. H. (1987) Lithium isotope analysis by thermal ionization mass spectrometry of lithium tetraborate. *Anal. Chem.* **59,** 2662–2665.

Clayton D. D. and Jin L. (1995) Gamma rays, cosmic rays, and extinct radioactivity in molecular clouds. *Astrophys. J.* **451,** 681–699.

Clayton D. D., Hartmann D. H., and Leising M. D. (1993) On ^{26}Al and other short-lived interstellar radioactivity. *Astrophys. J.* **415,** L25–L29.

Davis A. M. (2002) Lithium, beryllium and boron distributions in CAIs. *Meteoritics Planet. Sci.* **37,** A40 (abstr.).

Davis A. M., MacPherson G. J., and Hinton R. W. (1986) Rims revealed—ion microprobe analysis of individual rim layers in a Vigarano Type A inclusion. *Meteoritics* **21,** 349–351 (abstr.).

Davis A. M., Hinton R. W., and MacPherson G. J. (1987) Relict grains in a Vigarano refractory inclusion. *Meteoritics* **22,** 363–365 (abstr.).

Davis A. M., Simon S. B., Grossman L. (1994) Alteration of Allende Type B1 CAIs: When, where and how. *Lunar Planet. Sci. XXV,* 315–316. Lunar Planet. Inst., Houston (abstr.).

Fahey A. J., Zinner E. K., Crozaz G., and Kornacki A. S. (1987) Microdistributions of Mg isotopes and REE abundances in a Type A calcium-aluminum-rich inclusion from Efremovka. *Geochim. Cosmochim. Acta* **51,** 3215–3229.

Goswami J. N. and Vanhala H. A. T. (2000) Extinct radionuclides and the origin of the solar system. In *Protostars and Planets VI* (eds. V. Mannings, A. P. Boss, and S. S. Russell). Univ. of Arizona Press, Tucson, pp. 963–994.

Goswami J. N., Marhas K. K., and Sahijpal S. (2001) Did solar energetic particles produce the short-lived nuclides present in the early solar system? *Astrophys. J.* **549,** 1151–1159.

Goudis C. (1982) *The Orion Complex: A Case Study of Interstellar Matter,* Reidel, Dordrecht. 311 pp.

Gounelle M., Shu F. H., Shang H., Glassgold A. E., Rehm K. E., and Lee T. (2001) Extinct radioactivities and protosolar cosmic rays: Self-shielding and light elements. *Astrophys. J.* **548,** 1051–1070.

Gray C. M., Papanastassiou D. A., and Wasserburg G. J. (1973) The identification of early condensates from the solar nebula. *Icarus* **20,** 213–239.

Heymann D. and Dziczkaniec M. (1976) Early irradiation of matter in the solar system: Magnesium (proton, neutron) scheme. *Science* **191,** 79–81.

Huss G. R., Hutcheon I. O., and Wasserburg G. J. (1997) Isotopic systematics of presolar silicon carbide from the Orgueil (CI) chondrite: Implications for solar system formation and stellar nucleosynthesis. *Geochim. Cosmochim. Acta* **61,** 5117–5148.

Huss G. R., MacPherson G. J., Wasserburg G. J., Russell S. S., and Srinivasan G. (2001) Aluminum-26 in calcium-aluminum-rich inclusions and chondrules from unequilibrated ordinary chondrites. *Meteorit. Planet. Sci.* **36,** 975–997.

Krot A. N., Weber D., Greshake A., Ulyanov A. A., McKeegan K. D., Hutcheon I., Sahijpal S., Keil K. (1999) Relic Ca, Al-rich inclusions in chondrules from the carbonaceous chondrites Acfer 182 and Acfer 094. *Lunar Planet. Sci. XXX.* Lunar Planet. Inst., Houston. #1511 (abstr.).

Lee T., Shu F. H., Shang H., Glasswold A. E., and Rehm K. E. (1998) Protostellar cosmic rays and extinct radioactivities in meteorites. *Astrophys. J.* **506,** 898–912.

MacPherson G. J. (1985) Vigarano refractory inclusions: Allende unaltered and a possible link with C2 inclusions. *Meteoritics* **20,** 703–704 (abstr.).

MacPherson G. J. and Grossman L. (1984) "Fluffy" Type A Ca-, Al-rich inclusions in the Allende meteorite. *Geochim. Cosmochim. Acta* **48,** 29–46.

MacPherson G. J. and Davis A. M. (1993) A hibonite-perovskite-rich Type A Leoville inclusion. *Meteoritics* **28,** 389 (abstr.).

MacPherson G. J. and Huss G. R. (2001) Extinct ^{10}Be in CAIs from Vigarano, Leoville, and Axtell. Lunar Planet. Sci. XXXII. Lunar Planet. Inst., Houston #1882 (abstract).

MacPherson G. J., Hashimoto A., and Grossman L. (1985) Accretionary rims on inclusions in the Allende meteorite. *Geochim. Cosmochim. Acta* **49,** 2267–2279.

MacPherson G. J., Davis A. M., and Zinner E. K. (1995) The distribution of aluminum-26 in the early Solar System –A reappraisal. *Meteoritics* **30,** 365–386.

Mandzhavidze N., Ramaty R., and Kozlovsky B. (1999) Determination of the abundance of subcoronal ^{4}He and of solar flare-accelerated ^{3}He and ^{4}He from gamma-ray spectroscopy. *Astrophys. J.* **518,** 918–925.

McKeegan K. D., Chaussidon M., and Robert F. (2000) Incorporation of short-lived ^{10}Be in a calcium-aluminum-rich inclusion from the Allende meteorite. *Science* **289,** 1334–1337.

McKeegan K. D., Chaussidon M., Krot A. N., Robert F., Goswami J. N., Hutcheon I. D. (2001). Extinct radionuclide abundances in Ca, Al-rich inclusions from the CV chondrites Allende and Efremovka: A search for synchronicity. *Lunar Planet. Sci. XXXII.* Lunar Planet. Inst., Houston. #2175 (abstr.).

Pearce N. J. G., Perkins W. T., Westgate J. A., Gorton M. P., Jackson S. E., Neal C. R., and Chenery S. P. (1997) A compilation of new and published major and trace-element data for NIST SRM 610 and NIST SRM 612 glass reference materials. *Geostandards Newsletter* **21,** 115–144.

Podosek F. A. and Nichols R. H. Jr. (1997) Short-lived nuclides in the solar nebula. In *Astrophysical Implications of the Laboratory Study of Presolar Materials* (eds. T. J. Bernatowicz and E. K. Zinner), pp. 617–647. American Institute of Physics, Woodbury, NY.

Podosek F. A., Zinner E. K., MacPherson G. J., Lundberg L. L., Brannon J. C., and Fahey A. J. (1991) Correlated study of initial ^{87}Sr/^{86}Sr and Al-Mg isotopic systematics and petrologic properties in a suite of refractory inclusions from the Allende meteorite. *Geochim. Cosmochim. Acta* **55,** 1083–1110.

Reames D. V., Barbier L. M., von Rosenvinge T. T., Mason G. M., Mazur J. E., and Dwyer J. R. (1997) Energy spectra of ions accelerated in impulsive and gradual solar events. *Astrophys. J.* **483,** 515–522.

Reedy R. C. (1987) Nuclide production by primary cosmic-ray protons. *Proc. Lunar. Planet. Sci Conf 17th, J. Geophys. Res.* **92,** E697–702.

Reedy R. C. (1989) Cosmogenic-nuclide production rates in interstellar grains. *Lunar Planet. Sci. XX.* Lunar Planet. Inst., Houston. pp. 888–889 (abstr.).

Reeves H. (1994) On the origin of the light elements ($Z < 6$). *Rev. Mod. Phys.* **66,** 193–216.

Russell S. S. and Kearsley A. (1999) Relict refractory inclusions within chondrules from CV meteorites. *Meteorit. Planet. Sci.* **34,** A99–A100 (abstr.).

Russell S. S., Davis A. M., MacPherson G. J., Guan Y., and Huss G. R. (2000) Refractory inclusions from the ungrouped carbonaceous chondrites MacAlpine Hills 87300 and 88107. *Meteorit. Planet. Sci.* **35,** 1051–1066.

Shu F. H., Shang H., and Lee T. (1996) Toward an astrophysical theory of chondrules. *Science* **271,** 1545–1552.

Shu F. H., Shang H., Gounelle M., Glassgold A. E., and Lee T. (2001) The origin of chondrules and refractory inclusions in chondritic meteorites. *Astrophys. J.* **548,** 1029–1050.

Shukolyukov A. and Lugmair G. W. (1993) Live iron-60 in the early solar system. *Science* **259,** 1138–1142.

Srinivasan G., Huss G. R., and Wasserburg G. J. (2000) A petrographic, chemical and isotopic study of calcium-aluminum-rich inclusions and aluminum-rich chondrules from the Axtell CV3 chondrite. *Meteorit. Planet. Sci.* **35,** 1333–1354.

Sugiura N., Shuzou Y., and Ulyanov A. A. (2001) Beryllium-boron and aluminum-magnesium chronology of calcium-aluminum-rich inclusions in CV chondrites. *Meteorit. Planet. Sci.* **36,** 1397–1408.

Teshima J., Wasserburg G. J. (1985) Textures, metamorphism and origin of Type A CAI's. *Lunar Planet. Sci. XVI.* Lunar Planet. Inst., Houston. pp. 855–856 (abstr.).

Wark D. A., Lovering J. F. (1977) Marker events in the early solar system: Evidence from rims on Ca-Al-rich inclusions in carbonaceous chondrites. *Proc. Lunar Sci. Conf. 8th,* 95–112.

Wasserburg G. J., Lee T., and Papanastassiou D. A. (1977) Correlated oxygen and magnesium isotopic anomalies in Allende inclusions: II. *Magnesium. Geophys. Res. Lett.* **4,** 299–302.

Wasserburg G. J., Busso M., Gallino R., and Raiteri C. M. (1994) Asymptotic giant branch stars as a source of short-lived radioactive nuclei in the solar nebula. *Astrophys. J.* **424,** 412–428.

Woosley S. E. and Weaver T. A. (1995) The evolution and explosion of massive stars. II. Explosive hydrodynamics and nucleosynthesis. *Astrophys. J. Suppl.* **101,** 181–235.